PERFORMANCE ANALYSIS OF Si-NW BASED BIOSENSORS FOR DETECTION OF CHARGED BIOMOLECULES

Exam Roll: 6214; Session: 2009-10

Department of Applied Physics, Electronics and Communication Engineering

University of Dhaka

Submitted to the Department of
Applied Physics, Electronics and Communication Engineering
in partial fulfillment of the requirements for the degree of
Master's in science

University of Dhaka

2012

Disclaimer

This is to certify that the thesis work titled "*Performance analysis of Si-NW based biosensors for detection of charged biomolecules*" has been completed by Md. Obidul Islam, Master in Science student, Exam Roll 6214, Session 2009 –10, Department of Applied Physics, Electronics & Communication Engineering, Faculty of Engineering & Technology, University of Dhaka, under the supervision of Ms Ayesha Zaman, Lecturer, Department of Applied Physics, Electronics & Communication Engineering, Faculty of Engineering & Technology, University of Dhaka. Results and findings of this thesis have been obtained after rigorous work by the student and checked by then supervisor and no part of the result is taken from any other sources.

.....
Md. Obidul Islam
Exam Roll no.: 6214
Session: 2009-10

.....
Ms Ayesha Zaman
Lecturer,
Department of Applied Physics,
Electronics & Communication
Engineering, University of Dhaka

Acknowledgement

I first thank my supervisor, Ms Ayesha Zaman, for her relentless support, instruction and advice. Without her astute guidance, I could never have done this work. Even more importantly, her enthusiasm in innovations, attitude towards research and optimism deeply impressed and encouraged me.

I would like to thank research group at Purdue University, West Lafayette. Their response to my email regarding the device simulation in MATLAB was truly helpful.

I would also like to thank my friends, Mr. Mohiuddin Manna and Mr. Onirban Islam for their assistance in producing simulation results as presented in this thesis. Also, their comments on my thesis were especially enlightening.

Finally, special thanks to my family for their unlimited love, encouragement, and support.

Abstract

Nanoscale structures exhibit unique electrical and electrochemical properties, which has stimulated increasing interest in the application of biosensors. Biosensor based on Si-NW have already demonstrated ultrasensitive detection of DNA, proteins, pH levels, etc. and CNT based sensors have been used to detect NO_2 and interaction with protein. Despite these significant technological advances in nano sensors, it is somewhat surprising that the design principles of nano sensors are not well elaborated, and the path to further optimization is ill defined.

Although it is generally accepted that NWs with lower doping density and smaller diameter provides better sensitivity, the influence of factors like surrounding environment (air/water) and electrostatic screening due to the ions in the solution on NW sensor performance needs to be explained for the systematic optimization of sensor design. In this thesis a simple analytical model, based on reaction-diffusion theory is developed to predict the trade-off between average response time and minimum detectable concentration for Nano biosensors. Analytic solutions of Poisson–Boltzmann and diffusion-capture equations are explored to show that the electrostatic screening within an ionic environment limits the response of Si-NW based 2D cylindrical nano biosensor. All the analytical simulations are done by MATLAB program and the results are supported by the numerical simulations obtained from a simulation tool BioSensorLab.

This thesis analyzes various performance parameters for Si-NW based biosensors and their employment for the detection of biomolecules. After a critical analysis of the factors that currently limit the practical use of Si-NW based biosensors, this thesis concludes with an outline of potential future applications for silicon nanowires in biology and medicine.

Table of Contents

List of Tables

List of Figures

List of Symbols

N_0	-	Density of receptors on the sensor surface
N	-	Density of conjugated receptors
N_D	-	Doping density
N_{equi}	-	Equilibrium concentration of conjugated biomolecule
N_F	-	Density of surface functionalization groups
ρ_s	-	Concentration of analyte particles at the sensor surface at any given time
ρ_0	-	Equilibrium analyte concentration
k_F	-	Capture constant
k_R	-	Dissociation constant
D	-	Diffusion coefficient
L_{NW}	-	Nanowire length
a_0	-	Radius of nanowire
t_{OX}	-	Thickness of oxide layer
N_s	-	No. of analyte particles required to capture for detectable signal change
t_s	-	Settling time
$C_{D,SS}$	-	Diffusion equivalent capacitance

ε_{Si}	-	Dielectric constant of Silicon nanowire
ε_{ox}	-	Dielectric constant of oxide layer
ε_{w}	-	Dielectric constant of electrolyte
q	-	Charge of an electron
N_{avo}	-	Avogadro's number
I_0	-	Electrolyte concentration
k_B	-	Boltzmann constant
T	-	Absolute temperature
k	-	Debye- Hückel screening parameter
σ_T	-	Charge density due to analyte molecules on the sensor surface
σ_{NW}	-	Charge induced in the sensor
σ_{DL}	-	Net charge in the electrical double layer formed at the sensor surface
σ_S	-	Charge of a biomolecule
φ	-	Surface potential
G	-	Conductance
S	-	Sensitivity
μ	-	Mobility of the carriers
K_n	-	Modified Bessel function of the second kind of order n
K_a	-	Ionization constant

Chapter 1

INTRODUCTION

1.1 MOTIVATION

In recent years, electronic detection of biomolecules in the solvent is one of the widely studied topics in nanotechnology. Systems based on nanoscale devices can provide fast, low-cost, and high throughput analysis of biological processes and are gaining importance due to their large potential in commercial applications, ranging from detection of DNA, Protein, pH etc., to the discovery of new drug delivery systems [1].

Since the early 1970s, the basic idea of ion-sensitive field-effect transistor (ISFET) has been realized based on metal oxide silicon field-effect transistor (MOSFET) [2]. In an ISFET the gate structure of a MOSFET is replaced by a biomaterial layer (ion-selective layer), electrolyte and a reference electrode. The ISFET can measure the concentration of certain ion species in the electrolyte, such as protein, enzyme and DNA [3]. It was regarded as a low-cost alternative to traditional chemical sensors with potential for on-chip integration [4]. However, several disadvantages, such as lack of good solid state electrodes, parasitic sensitivity to temperature and light, time dependent instability of sensor parameters, have restrained the development of ISFET as a popular biosensor technology [5].

Instead, over the years, the chemical sensors have adopted fluorescent labeling and parallel optical detection techniques for fast detection of biomolecules at relatively low concentrations (e.g., DNA microarray [6]). Although these fluorescence-based sensors are now widely used, they still require expensive and time-consuming preprocessing and postprocessing for sample preparation and data analysis. Moreover, DNA microarrays are not sensitive enough to allow measurement of critical substances that may occur at very low

concentration or that are in rapid flux. It is in this context, direct label-free electronic sensing of biomolecules using nanoscale biosensors becomes significant.

Label-free schemes detect the presence of target biomolecules based on their intrinsic characteristics (e.g., field-effect transistor (FET) biosensor is a charge based detection scheme), not through the presence of extrinsic labels (e.g., magnetic nanoparticle or fluorophore) attached to the target molecule in a previous labeling step. The significant technological advances in silicon very-large-scale-integration (VLSI) have made fabrication of Si-NW biosensors possible. These biosensors consist of a Si-NW core, a surrounding silicon oxide layer, a layer of biomaterial, and surface receptor biomolecules. The specific binding of a few charged target biomolecules onto the receptor molecules can modulate the carriers' distribution inside the Si-NW. Because of the small size and large surface-to-volume ratio of the Si-NW, the detecting sensitivity is increased as compared with traditional ISFET biosensors [1].

Si-NW biosensors have already demonstrated ultrasensitive detection of DNA, proteins, pH levels, etc. Thus, it is possible that arrays of such sensors will be able to detect a huge class of biomolecules. The major advantage of Si-NW biosensors is the label free operation, as opposed to the expensive and time-consuming preprocessing and postprocessing for sample preparation and data analysis in chemical detection. Other advantages include the high sensitivity and the real time and continuous operation.

Among the demonstrated experiments, as DNAs are highly charged biomolecule the detection of DNA is of special interest and is widely demonstrated as a model system to study biorecognition with other biomolecules [1]. For target DNA detection using ss DNA as receptors, the ion concentration of the solution has to be quite high to ensure the conjugation between the negatively charged target and receptor strands. For DNA detection, receptor molecules should be uncharged, and PNA (peptide nucleic acid) should be a better candidate as receptor than complimentary ss DNA molecules, which is consistent with the experimental trends in recent literature [7], [8].

Despite these promising experimental results of Si-NW biosensors and their enormous potential in commercial applications, it is somewhat surprising that the fundamental mechanism of electrical sensing of biomolecules and the design principles of Si-NW

biosensor remain poorly understood. Many researchers of nanometer-scale phenomena focus on the fact that miniaturizing a sensor often increases its signal-to-noise ratio (S:N), an inherent advantage for signal transduction, but the effect of nanoscale miniaturization on the overall sensitivity, which includes mass transport effects, has not been widely considered [9]. Many parameters affect the performance of Si-NW biosensor, such as the dimension of the Si-NW, the doping density of the Si-NW, the surrounding environment (the ions concentration in the solvent). These parameters need to be investigated for the systematic optimization of biosensor design.

In this thesis, a comprehensive modeling theory and simulation approach is proposed to account for the underlying electrical detection mechanism of DNA using Si-NW biosensor. The theory is based on self-consistent solution of the diffusion-capture model and Poisson Boltzmann equation. The D-C equations are solved numerically and analytically to explore the performance limits of nanosensors. The Poisson Boltzmann equation is derived from the classical Poisson equation using the Boltzmann distribution to model the charge distribution in the ionic solvent. The analytical solution to the Poisson Boltzmann equation is discussed to illustrate the importance of screening-limited kinetic response of Si-NW sensor. The detailed structures, modeling procedure and simulation methods of the Si-NW biosensor are presented. The simulation results are analyzed and the influence of parameters like the dimension of the Si-NW, the doping of the Si-NW, and surrounding environment (the ions concentration in the solvent) are investigated for the performance optimization of the Si-NW biosensor. All approximate analytical solutions are checked against exact numerical solutions for accuracy.

1.2 LAYOUT OF THESIS

This thesis consists of six chapters beginning with this chapter. Chapter 1 gives a brief background as well as the layout of this thesis.

Chapter 2 presents an overview of biosensor application. The basic operation principle of different types of biosensor is discussed here.

Chapter 3 is dedicated to Si-NW biosensor. This chapter discussed the background of Si-NW, its basic structure as well as its properties that make it unique in biosensor application. Growth technique of this sensor is presented briefly to give an idea of how these devices can be fabricated in laboratory. Also various performance parameters (settling time, sensitivity and selectivity) of Si-NW biosensor are defined in this chapter.

Chapter 4 deals with the basis of research of this thesis. The comprehensive modeling theory and simulation approach are presented to account for the underlying detection mechanism of DNA using Si-NW biosensor. This chapter is divided into two parts. The first part introduces the diffusion-capture model and analytical solutions of model equations for estimating the minimum detectable concentration of target biomolecules. The second part focuses on the derivation of Poisson-Boltzmann equation. Poisson-Boltzmann equation is derived from the classical Poisson equation using the Boltzmann distribution to model the charge distribution in the ionic solution. Analytical solutions of the Poisson-Boltzmann equation for three special cases are discussed. Also, several popular numerical methods for solving the Poisson-Boltzmann equation are introduced.

Chapter 5 deals with the simulation results with detailed analysis. The influence of parameters like the dimension of the Si-NW, the doping of the Si-NW, and surrounding environment (the ions concentration in the solvent) are investigated for the performance optimization of the Si-NW biosensor.

Finally chapter 6 draws the conclusions and summarizes the accomplishments of this work. The potential application of this research and possible future work are included.

Chapter 2

OVERVIEW OF BIOSENSOR

2.1 BASIC CONCEPT OF BIOSENSORS

A biosensor is an analytical device consisting of an immobilised layer of biological material (engyme, antibody, organelle, hormones, nucleic acids or whole cells) in the intimate contact with a physical component (transducer) whice analyzes the biological signal and converts into an electrical signal. The name"biosensor" signifies that the device is a combination of two parts:

- bio-element
- sensor-element.

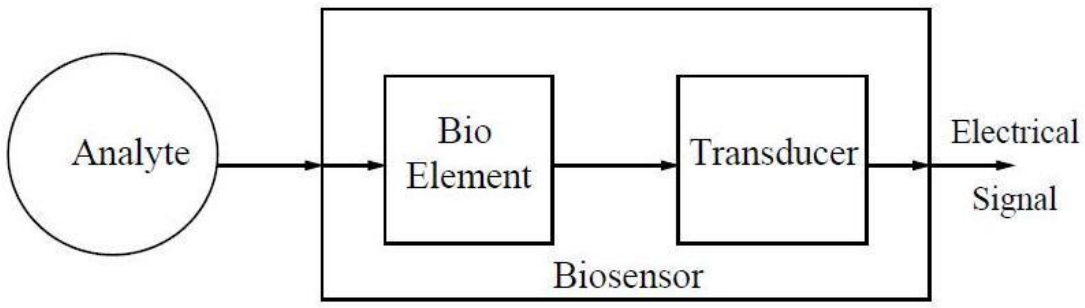

Figure 2.1.1: Basic Concepts of Biosensor

The basic concepts of biosensor can be illustrated by the help of Fig. 2.1.1. A specific"bio" element (say, nucleic acid) recognizes a specific analyte and the"sensor" element transduces the change in the biomolecule into electrical signal. The bio element is very specific to the analyte to which it is sensitive. It does not recognize other analytes. A detailed list of different possible bio-elements and sensor-elements is in Fig. 2.1.2.

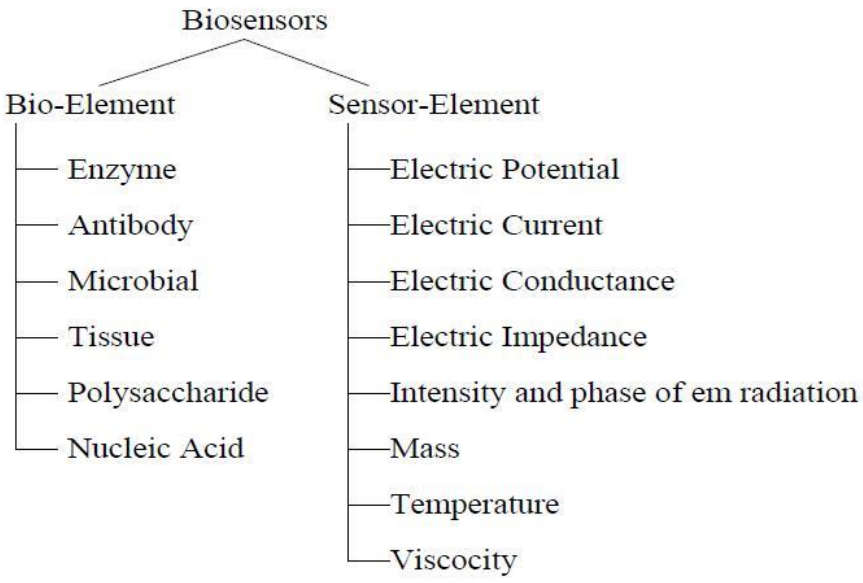

Figure 2.1.2: Elements of a Biosensor

2.2 HISTORY OF BIOSENSORS

The history of biosensors started in the year 1962 with the development of enzyme electrodes bythe scientist Leland C. Clark. Since then the research communities from various fields like VLSI, physics, chemistry, material science, and so on, have come together to develop more sophisticated, reliable and matured biosensing devices for applications in the fields of medicine, agriculture, and biotechnology, etc. In 1970 the ISFET was first demonstrated by Bergveld. In 1972, for the first time Yellow Springs Instruments Co., USA developed a biosensor for diagnostic purposes for measuring glucose in blood plasma. It is a hand-held machine which measures six components of blood plasma (glucose, urea, nitrogen, sodium, potassium and chloride). Table 1 lists the history of biosensors in brief.

Year	Events
1916	First report on the immobilization of proteins: adsorption of invertaseon activated charcoal -Nelson and Grif.
1922	First glass pH electrode.
1956	Invention of the oxygen electrode (Clark).
1962	First description of a biosensor: an amperometric enzyme electrode for glucose (Clark).
1969	First potentiometric biosensor: urease immobilized on an ammonia electrode to detect urea.
1970	Invention of the Ion-Selective Field-Effect Transistor (ISFET) (Bergveld).
1972	First commercial biosensor: Yellow Springs Instruments glucose biosensor (pen shaped single use electrode).
1975	First microbe-based biosensor. First immunosensor: ovalbuminon a platinum wire. Invention of the pO2/pCO2 optode (fluorescence signal & gaspermeable membrane usage).
1980	First fibreoptic pH sensor for in vivo blood gases (Peterson).
1982	First fibre optic-based biosensor for glucose.
1983	First surface plasmon resonance (SPR) immunosensor.
1984	First mediated amperometric biosensor: ferrocene used with glucose oxidase for the detection of glucose.
1987	Launch of the MediSenseExacTech™ blood glucose biosensor (strips/pen modeland disposable).
1990	Launch of the Pharmacia BIACore SPR-based biosensor system.
1992	i-STAT launches hand-held blood analyzer.
1996	Glucocard launched. Abbott acquires MediSense for $867 million.
1998	Launch of LifeScan FastTake blood glucose biosensor. Merger of Roche and Boehringer Mannheim to form Roche Diagnostics.
2001	LifeScan purchases Inverness Medical's glucose testing business for $1.3billion.
1999 to now	BioNMES, Quantum dots, Nanoparticles, Nanocantilever, Nanowire and Nanotube.

Table 1: History of biosensors

2.3 BASIC PRINCIPLE OF BIOSENSORS

The principle of biosensor is quite simple. Figure 2.3.1 represents a schematic outline for a general biosensor. The biological material is immobilized on the immobilization support (a permeable membrane) in the direct vicinity of a transducer. The substances to be measured interact with the immobilized material and yield a product. The product may be heat, gas (Oxygen), electrons, hydrogen ions or the product of ammonium ions. The product passes through another membrane to the transducer. The transducer converts product into an electric signal which is then amplified. The signal processing equipments convert the amplified signal into a display most commonly the electric signal which can be read out and recorded.

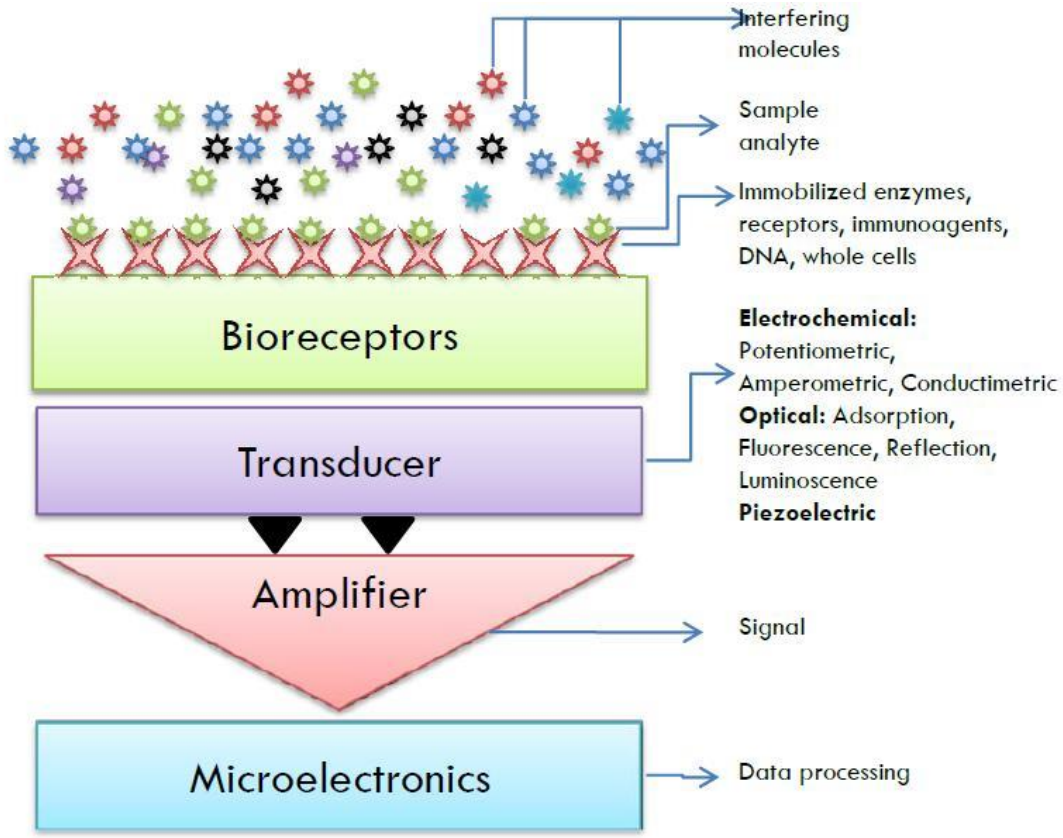

Figure 2.3.1: Generalized outline for a biosensor

2.4 TYPES OF BIOSENSORS

2.4.1 ELECTROCHEMICAL BIOSENSORS

Electrochemical biosensors are mainly used for detection of hybridized DNA, DNA-binding drugs, glucose concentration, etc. The underlying principle for this class of biosensors is that many chemical reactions produce or consume ions or electrons which in turn cause some change in the electrical properties of the solution which can be sensed out and used as measuring parameter [10]. These types of biosensors use electronic devices such as field effect transistors that measures charge accumulation on their surface. The field effect transistors can be modified to ion sensitive, enzyme sensitive or antibody sensitive ones by using selective ions, enzymes or antibodies respectively. Figure 2.4.1 depicts the basic working principle of an electrochemical biosensor.

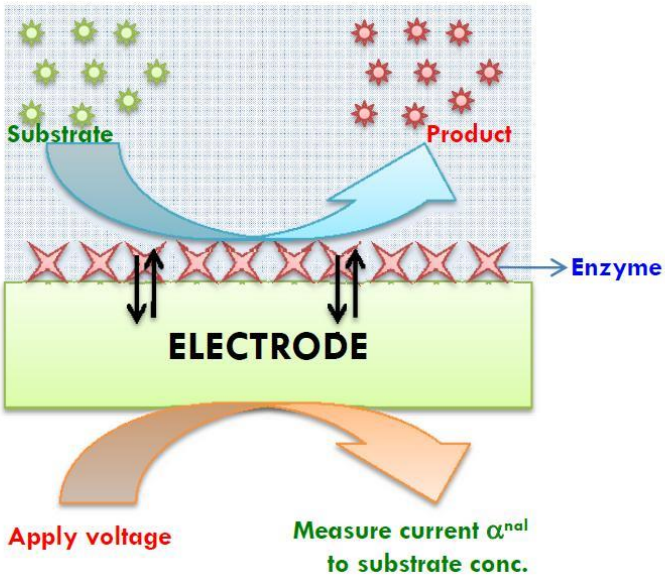

Figure 2.4.1: Schematic of an electrochemical biosensor

Based on their operating principle, the electrochemical biosensors can employ potentiometric, amperometric and impedimetric.

2.4.1.1 POTENTIOMETRIC BIOSENSORS

Potentiometric biosensors are based on ion-selective electrodes (ISE) and ion-sensitive field effect transistors (ISFET). The ISFET sensing principle is based on the charge adsorption at the ion-solid interface between the sensing layer which contains hydroxyl groups and the electrolyte, from which hydroxyls may accept or donate protons [11]. In this process a double-layer capacitance is created with a potential drop, which influences the threshold voltage of the transistor depending on the value of H^+ (protons) concentration (pH). The structure of the ISFET is presented by a cross-section in Figure 2.4.2.

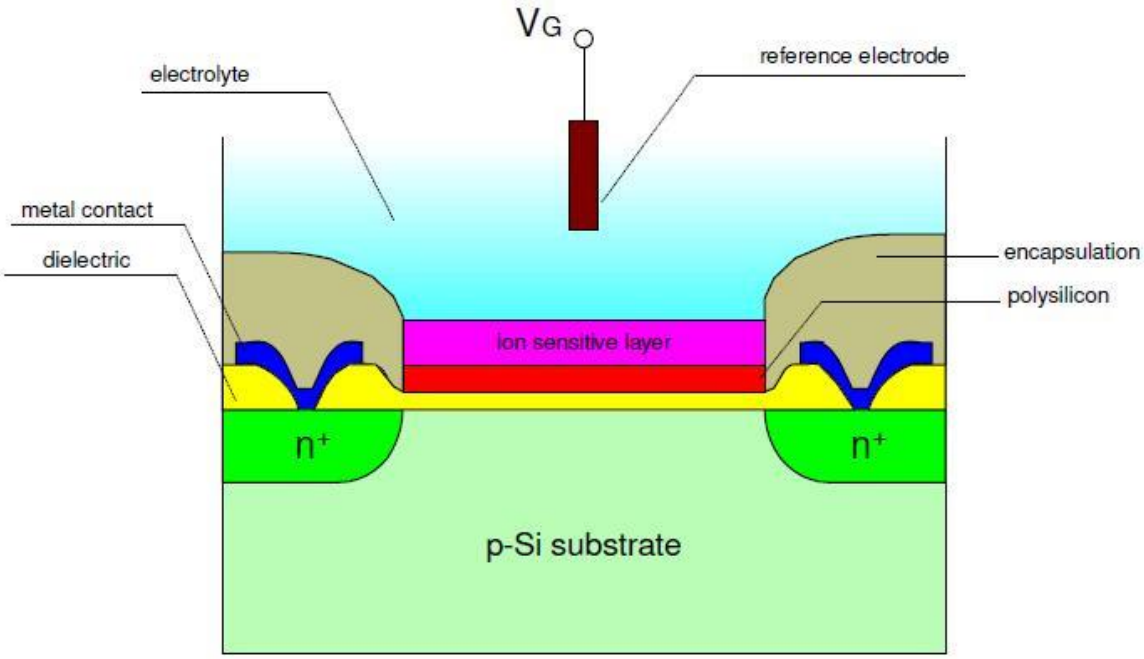

Figure 2.4.2: The structure of an ISFET

2.4.1.2 AMPEROMETRIC BIOSENSORS

Amperometric Biosensors produce a current proportional to the concentration of the substance to be detected. The most common amperometric biosensors use the Clark Oxygen electrode.

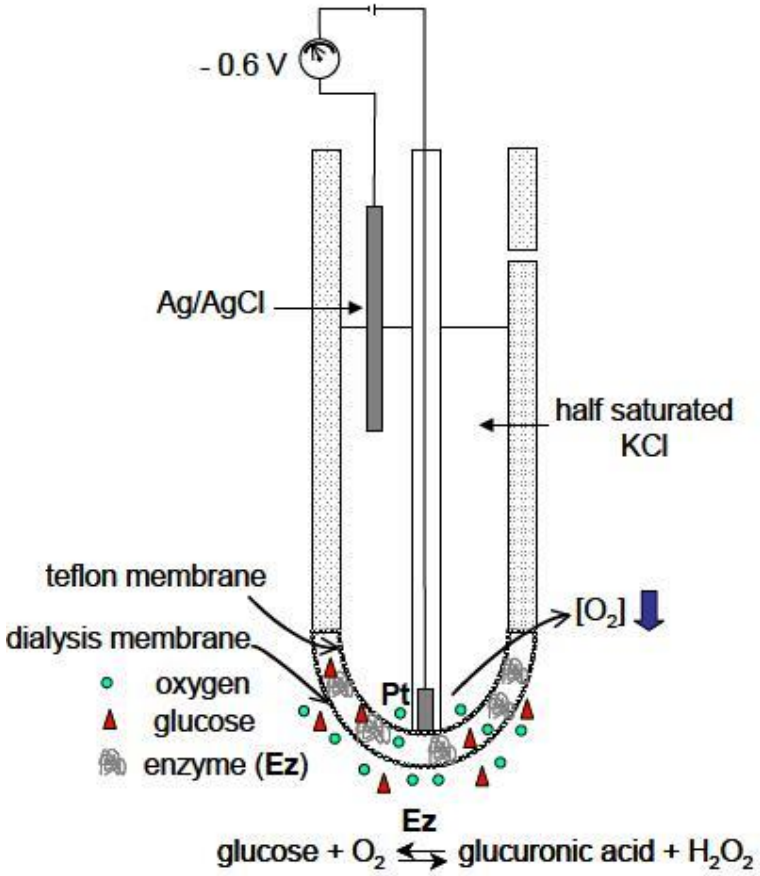

Figure 2.4.3: Glucose Amperometric Biosensor

In the glucose Amperometric Biosensor (Figure 2.4.3), the Clark Oxygen electrode is separated from glucose by a membrane, that is permeable to oxygen. A biocatalyst Glucose Oxidase (GOD) is housed between this membrane and another membrane that separates it from the glucose. This membrane that separates GOD and glucose is permeable to both Oxygen and Glucose. In effect, the enzyme GOD is immobilized between two membranes, the top being permeable only to oxygen and the bottom to both Oxygen and Glucose.

2.4.1.3 IMPEDIMETRIC BIOSENSORS

The impedance biosensors include two electrodes with applied alternating voltage; amplitudes from a few to 100 mV are used. The impedance biosensor is commonly a functional part of the Wheatstone bridge. These systems are considered for the assay of urea when urease is used as a biorecognition component. Impedimetric biosensors are less frequent compared to potentiometric and amperometric biosensors; nevertheless, there have been some promising approaches. Hybridization of DNA fragments has been monitored by an impedance Assay. A model impedance immunosensor containing electrodeposited polypyrrole film with captured avidin connected through biotin to anti-human IgG was able to detect antibodies as low as 10 pg/ml. The ethanol level in some alcoholic beverages was evaluated by an impedance biosensor with immobilized yeast.

2.4.2 OPTICAL BIOSENSORS

2.4.2.1 OPTICAL FIBRE BIOSENSORS

Fiber-optic biosensors (FOB) are capable of real-time detection with a potential for specific sensitivity. Optical fiber biosensors can be used in combination with different types of spectroscopic technique, e.g. absorption, fluorescence, phosphorescence, Raman, surface Plasmon resonance (SPR), etc. The principle of FOBs is based on the total internal reflection fluorescence (TIRF) [12]. The technique is rooted in the fact that a fiber optic consists of a plastic or glass core surrounded by a layer of cladding material. Both components have different densities, hence light can be transmitted based on the principle of total internal reflection, which occurs when light propagating in a dense medium meets an interface with a less dense medium and is reflected. As it does so, some of the incident light propagates a short distance generating an evanescent wave (EW) on the outer side of the fiber interface. This EW can be used to excite fluorophores in the sample medium that are trapped on the fiber.

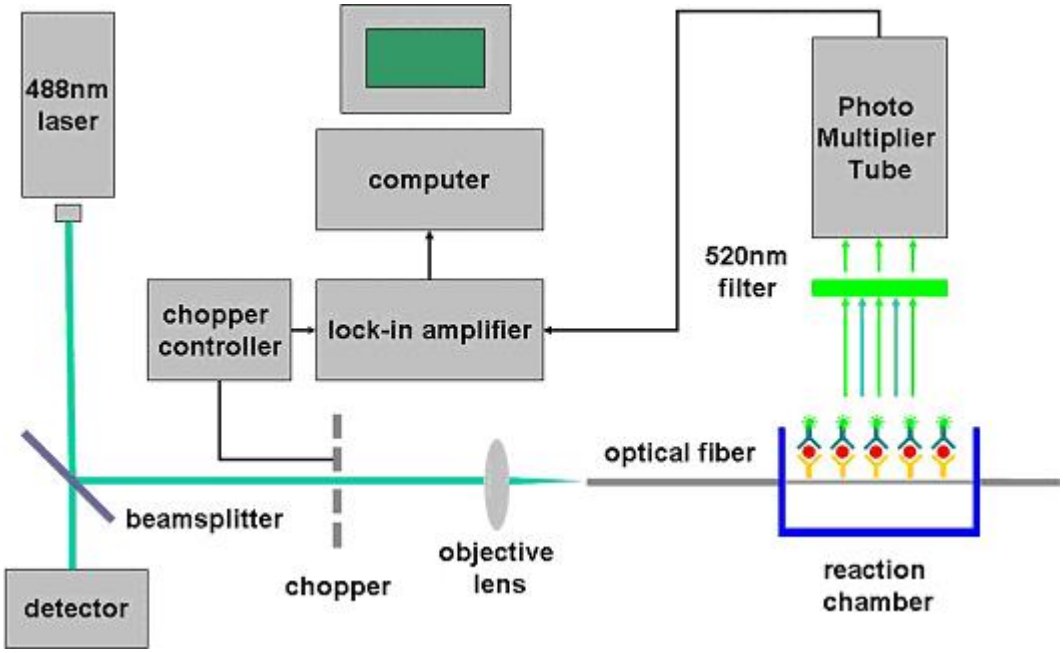

Figure 2.4.4: Setup and configuration of a fiber-optic biosensor. The fluorescence resulting from sample excitation by the evanescent wave generated in the near-field region of the fiber-core surface is detected by a photomultiplier tube placed perpendicularly to the fiber wall axis. This allows the fluorescence signal to be collected more efficiently.

2.4.2.2 FLUORIMETRIC BIOSENSORS

Fluorescence is a property present in certain molecules, called fluorophores, in which they emit a photon shortly after absorbing one with a higher energy wavelength. Most biological matter is fluorescent including the green fluorescent protein (GFP), nucleic acids, flavine nucleotides and NADH. NADH is fluorescent, while NAD+ is not as a result; all enzymatic reactions based on NAD/NADH are amenable to fluorescence analysis.

2.4.2.3 CALORIMETRIC BIOSENSORS

Many enzyme catalysed reactions are exothermic, generating heat which may be used as a basis for measuring the rate of reaction and, hence, the analyte concentration. This represents the most generally applicable type of biosensor. The temperature changes are usually determined by means of thermistors at the entrance and exit of small packed bed columns containing immobilised enzymes within a constant temperature environment (Figure 2.4.4).

Under such closely controlled conditions, up to 80% of the heat generated in the reaction may be registered as a temperature change in the sample stream. This may be simply calculated from the enthalpy change and the amount reacted.

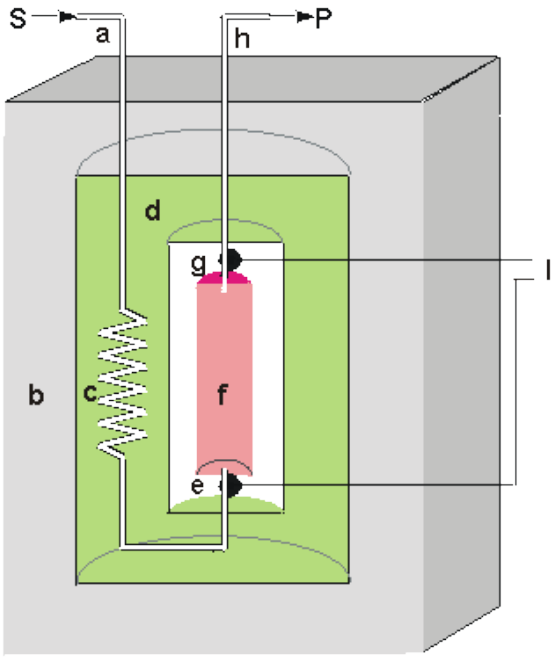

Figure 2.4.5: Schematic diagram of a calorimetric biosensor. The sample stream (a) passes through the outer insulated box (b) to the heat exchanger (c) within an aluminium block (d). From there, it flows past the reference thermistor (e) and into the packed bed bioreactor (f, 1ml volume), containing the biocatalyst, where the reaction occurs. The change in temperature is determined by the thermistor (g) and the solution passed to waste (h). External electronics (l) determines the difference in the resistance, and hence temperature, between the thermistors.

2.4.3 PIEZOELECTRIC BIOSENSORS

Piezoelectric sensors utilize crystals which undergo an elastic deformation when an electrical potential is applied to them. An alternating potential (A.C.) produces a standing wave in the crystal at a characteristic frequency. This frequency is highly dependent on the elastic properties of the crystal, such that if a crystal is coated with a biological recognition element the binding of a (large) target analyte to a receptor will produce a change in the resonance frequency, which gives a binding signal. In a mode that uses surface acoustic waves (SAW),

the sensitivity is greatly increased. This is a specialized application of the Quartz crystal microbalance as a biosensor.

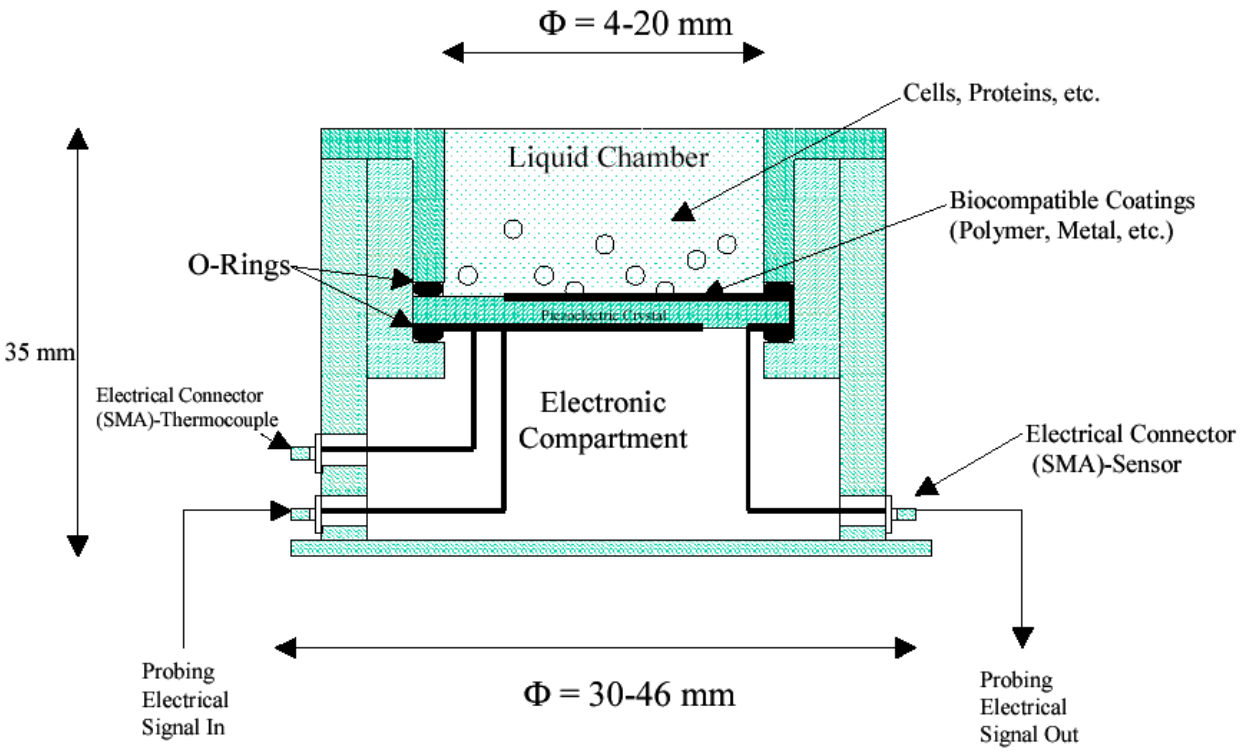

Figure 2.4.6: A piezoelectric transducer with biological sensing layer.

2.4.4 NANOBIOSENSORS

2.4.4.1 QUANTUM DOT BIOSENSORS

Quantum dots are nanometre-scale semiconductor crystals with unique optical properties that are advantageous for the development of biosensors. The surface chemistry of luminescent quantum dots has encouraged the development of multiple probes based on linked recognition molecules such as peptides, nucleic acids or small-molecule ligands. The detection of protein biomarkers can be done with an optical multiplexing approach using

quantum dots that generate a much more powerful fluorescent signal which provides a large increase in sensitivity compared to conventional dye particles. Quantum dots are also available in multiple colors, allowing the investigators to tag each antibody with a uniquely colored quantum dot.

Quantum dot-based FRET (Fluorescence Resonance Energy Transfer) technique is suitable for multiplexed ultrasensitive detection [13]. Single-particle analysis of biosensors that use energy transfer show analyte-dependent switching of nanoparticle emission from off to on. By monitoring the same nanoparticles under various conditions, a single charge-transfer-based biosensor shows a dynamic range for analyte (maltose) detection spanning from 100 pM to 10 μM while the emission intensities increase from 25 to 175% at the single-particle level.

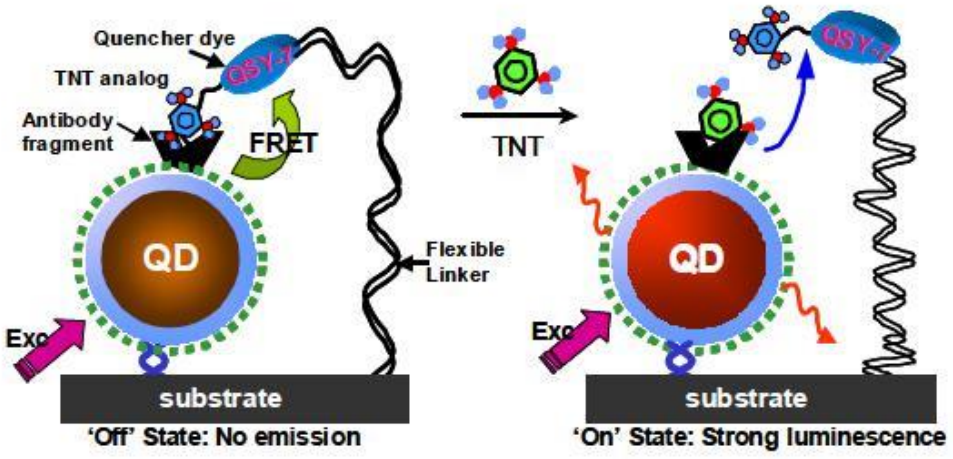

Figure 2.4.7: QD nanoscale TNT sensor based on Fluorescence Resonance Energy Transfer (FRET)

2.4.4.2 NANOWIRE BIOSENSORS

Nanostructures, such as nanowires (NWs) offer unique opportunities to develop novel sensors. The diameter of nanowire is comparable to those of the biological and chemical species being sensed. Therefore, Devices based on nanowires are emerging as a powerful platform for the direct detection of biological and chemical species. The combination of tunable Conducting properties of semiconducting NWs and the ability to bind analytes on

their surface yields direct, label-free electrical readout, which is exceptionally attractive for many applications.

Based on electrostatics considerations, it is known that two dimensional (2D) cylindrical nanowires are more sensitive to adsorbed charges (e.g., DNA, protein, etc.) compared to one dimensional (1D) planar ion-sensitive field effect transistor (ISFET) or chemical field-effect transistor. Due to the small size and large "surface to- volume ratio" of silicon nanowires (Si-NW), the presence of a few charged biological macromolecules on their surface can modulate the carrier distribution over their entire cross-sectional conduction pathway. This can result in an increased sensitivity as compared to traditional ISFET or chemical field-effect transistor sensors. Figure 2.4.8 represents a schematic of a Si-NW biosensor. The NW surface is functionalized with specific receptors to the targets. Surrounding fluid (air/water) interacts with the nanowire over the entire length and form a native oxide layer. The conductance of NW changes as the target molecules are captured by the receptor [14].

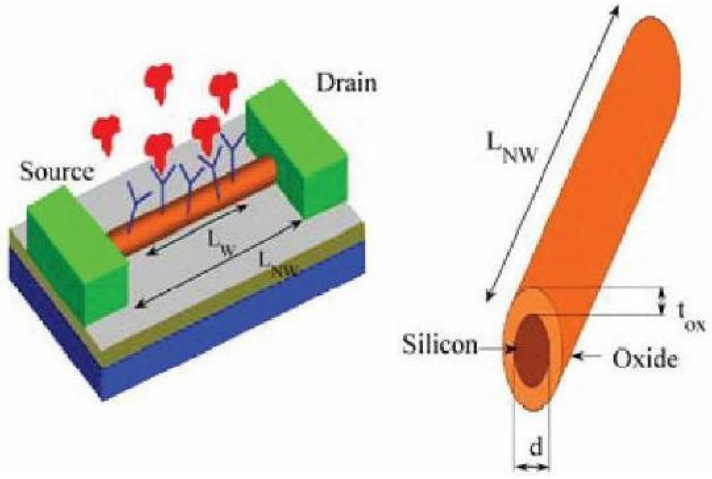

Figure 2.4.8: Schematic of a NW biosensor

2.4.4.3 NANOTUBE BIOSENSORS

The nanotube biosensor proved capable of detecting human ferritin, the primary iron-storing protein of cells, and E7 oncoprotein derived from human papillomavirus. A single walled carbon nanotube (SWNT) based biological sensor can detect biomolecules like Streptavidin and IgG. SWNTs have been employed for two types of sensing mechanisms: changes in the electrical conductance of the carbon nanotube matrix on non-covalent binding of

biomolecules to the side walls of the carbon nanotubes; quantification of mass uptake of the matrix on biomolecule incubation. Both sensing mechanisms exhibit consistent and highly sensitive responses. Bimolecular immobilization on the carbon nanotube surface was monitored by atomic force microscopy.

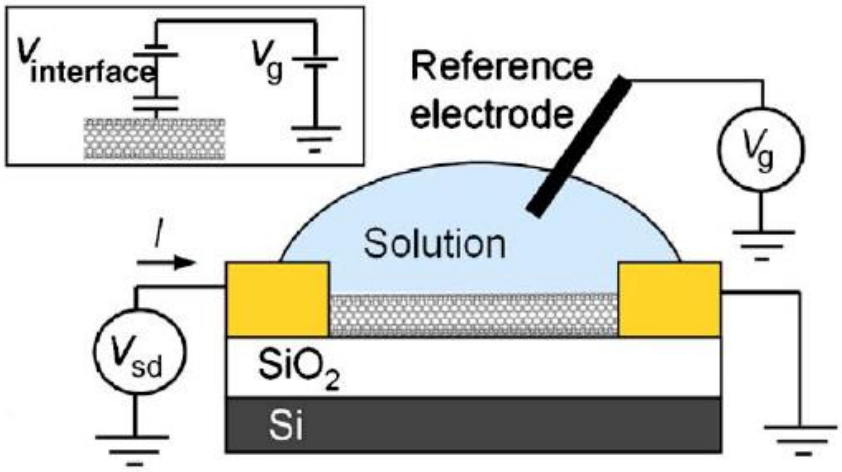

Figure 2.4.9: Schematic depiction of a CNT biosensor

Carbon nanotube transistors show tremendous potential for electronic detection of biomolecules in solution. The adsorption of biomolecules on the sidewall of a semiconducting carbon nanotube (CNT) causes changes in local electrostatic environment, thereby changing the conductance of the nanomaterial [15]. Carbon nanotube biosensors are generally constructed as shown in Figure 2.4.9. The device is exposed to solution, allowing protein adsorption on the semiconducting CNT. A metal wire is used to control the electrostatic potential of the solution. A gate voltage *Vg*, applied to the metal wire, can tune the conductance of the CNT, while a small bias is used to monitor the CNT conductance. The electrostatic potential difference between the solution and the CNT is determined by the applied gate voltage *Vg* and the interface potential at the metal-liquid interface. This interface potential depends sensitively on electrochemical reactions occurring at the metal-liquid interface.

2.4.4.4 NANOSPHERE BIOSENSORS

Nanosphere biosensor exhibit high sensitivity when immersed in an analyte solution. The diffusion of analyte particles towards the nanosphere is three dimensional. NiO hollow nanospheres are a promising material to construct glucose biosensors and enzyme biosensors. NiO hollow nanospheres were synthesized by controlled precipitation of metal ions with urea using carbon microspheres as templates, which were for the first time adopted to construct a novel amperometric glucose biosensor. Glucose oxidase was immobilized on the surface of hollow nanospheres through chitosan-assisted cross-linking technique. Due to the high specific active sites and high electrocatalytic activity of NiO hollow nanospheres, the constructed glucose biosensors exhibited a high sensitivity.

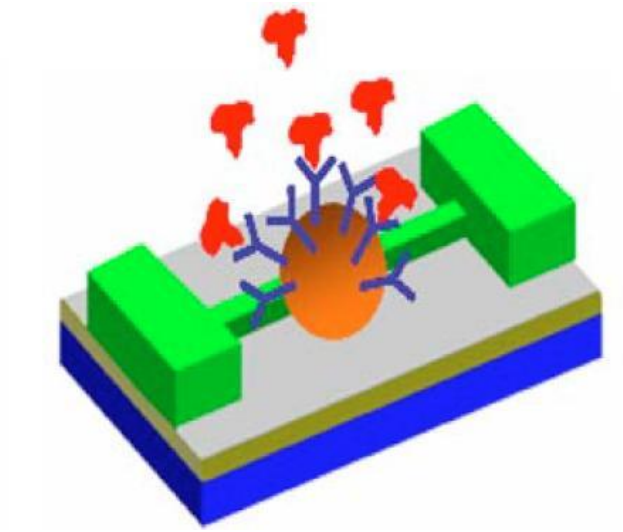

Figure 2.4.10: Schematic of a nanosphere biosensor

2.5 BIOSENSOR APPLICATIONS

There are many potential applications of biosensors of various types. Some examples are given below:

- A biosensor coupled with oxygen electrode and immobilized *Trichosporon cutaneum* is used for measuring Biological Oxygen Demand (BOD).

- The whole cell biosensor developed by immobilizing *Salmonella typhimurium* and *Bacillus subtilis* in conjugation with oxygen electrode can be used to measure mutagenicity and carcinogenicity of several chemical compounds.

- Ion sensitive field effect transistor (ISFET) based biosensors can measure the odour, freshness and taste of food. In determining fish freshness either ATPase, aminoxidase or putrescine oxidase is used. As ATP is not present in staled food, therefore signal do not occure.

- Miniaturization of ISFET sensors provides an ability of embedding into medical tools for continuous in-vivo measurements. Some examples of such integration in a catheter for measurements in CSF fluid for brain monitoring [2].

- A monolithically integrated ISFET sensor array includes the following applications:
    - pH detection by statistical distribution observing time and space fluctuations;
    - DNA detection using thiol-modified or saline-coupled oligonucleotides;
    - Bio-image sensing by converting photons to electrons using Photosystem I of *Thermosynechococcus elongatus*, and sensing the converted electric charges by ISFETs.

- Immunosensors have a wide range of applications in food, environment, pharmaceutical, chemistry and clinical diagnostics:
    - Gold nanoparticles (AuNPs)-based immunosensors can detect the *Escherichia coli* in milk samples.
    - Optical AuNPs-based DNA biosensor can be found in the genetically modified organisms (GMO) analysis.
    - DNA-AuNPs optical biosensor is related to the detection and quantification of pathogens such as *Helicobacter pylori*, which is a bacterium that colonizes the human stomach and causes major diseases such as gastritis, peptic ulcers and stomach cancer.

- A potentiometric biosensor with a molecularly imprinted polymer constructed for the herbicide atrazine assay. Another potentiometric biosensor with co-immobilized urease and creatinase on the poly (vinylchloride) ammonium membrane was used for creatine analysis.

- The amperometric biosensors are often used on a large scale for analytes such as glucose, lactate and sialic acid.

- Biosensors based on AChE and Butyrylcholinesterase (BChE) can be employed forrapid detection of organophosphates and carbamates (Skládal 1996) due to strong enzyme inhibition.

- Hybridization of DNA fragments amplified by a polymerase chain reaction has been monitored by an impedance immunosensor. The ethanol level in some alcoholic beverages was evaluated by an impedance biosensor with immobilized yeast.

- Si-NW sensors are demonstrated for direct, ultrasensitive detection of DNA, proteins, pH levels, etc.

- CNT-based sensors have been used to detect NO2 and interaction with protein.

- Nano-structured ZnO film based STD sensor is used to detect bacterial sexually transmitted disease Gonorrhoea.

- Nano-structured biosensor will have potential to protect the public from food borne illness, reduce the health risk of microbial contamination, strengthen food safety measures, and improve bioterrorism surveillance.

Chapter 3

Si-NW SENSOR AND BIOMOLECULE STRUCTURE

3.1 BACKGROUND

Ultrafast detection of biomolecules is one of the widely researched topics in nanotechnology. Nano-structured biosensor can provide fast, low-cost, and high-throughput analysis of biological
processes and promise to revolutionize many areas in medicine and biochemistry, ranging from the detection and diagnosis of diseases to the discovery of new drug delivery systems.

Since the early 1970s, microelectronic sensors based on thin film transistors and ion-sensitive field-effect transistors (ISFETs) have been explored as a low-cost alternative to traditional chemical sensors with potential for on-chip integration [4]. However, lack of good solid-state electrodes, parasitic sensitivity to temperature and light, time-dependent instability of sensor parameters, etc., have hindered their development as a disruptive biosensor technology [5]. Instead, over the years, the chemical sensors have adopted fluorescent labeling and parallel optical detection techniques for fast detection of biomolecules at relatively low concentrations. An example of such fluorescent based biosensor is the DNA microarray. Although these fluorescence-based sensors are now widely used, they still require expensive and time-consuming preprocessing and postprocessing for sample preparation and data analysis. Moreover, DNA microarrays are not sensitive enough to allow measurement of critical substances that may occur at very low concentration or that are in rapid flux. It is in this context, direct label-free electronic sensing of biomolecules using nanoscale biosensors becomes significant.

3.2 PROPERTIES OF NANOWIRE

Nanowires can be defined as structures that have a thickness or diameter of the order of a nanometer (10^{-9} meters). Nanowires have many interesting properties that are not seen in bulk or 3-D materials. This is because electrons in nanowires are quantum confined laterally and thus occupy energy levels that are different from the traditional continuum of energy levels or bands found in bulk materials.

Because of the enhanced surface to volume ratio of nanowires, their transport behavior may be modified by changing their surface conditions.

Transport properties for nanowires in the classical finite size and quantum size regimes, are highly diameter-dependent.

Some nanowires are **ballistic conductors**. Ballistic transport phenomena are usually observed in very short quantum wires, where the electron mean free path is much longer than the wire length and the conduction is a pure quantum phenomenon. In ballistic conductors, the electrons can travel through the conductor without collisions. Nanowires could conduct electricity efficiently without the byproduct of intense heat.

Nanowires with lengths much larger than the carrier mean free path, the electrons (or holes) undergo numerous scattering events when they travel along the wire. In this case, the transport is in the diffusive regime, and the conduction is dominated by carrier scattering within the wires.

Experiments show that the thermal conductivity of small homogeneous nanowires may be more than one order of magnitude smaller than in the bulk, arising mainly from strong boundary scattering effects and phonon confinement effects may eventually become important at still smaller diameter nanowires.

Due to the sharp density of states at the 1D subband edges, nanowires are expected to exhibit enhanced Seebeck coefficients compared to their bulk counterparts.

By applying a magnetic field to nanowires at very low temperatures (· 5 K), one can induce a transition from a 1D confined system at low magnetic fields to a 3D confined system as the field strength increases.

Lower doping density and smaller diameter makes nanowire highly sensitive to nanoscale biomolecule.

Nanowires can be manufactured using top-down approach [16].

3.3 PRINCIPLE OF Si-NW BIOSENSOR

Among several types of semiconducting nanowires (silicon nanowires, germanium nanowires, and GaAs nanowires), silicon nanowires (Si-NWs) are the most popular one because they can be easily synthesize and doped, and the silion/silicon-oxide interface in very stable. The configuration and the underlying detection mechanism of Si-NW biosensor are similar to that of a Si-NW FET. A Si-NW FET, whose conductance is modulated by an applied gate voltage, is transformed into a biosensor by modifying the silicon oxide surface with a layer of biomaterial, and surface receptor biomolecules. The binding of a charged biomolecules (target biomolecules) to the gate dielectric is analogous to applying a voltage using a gate electrode.

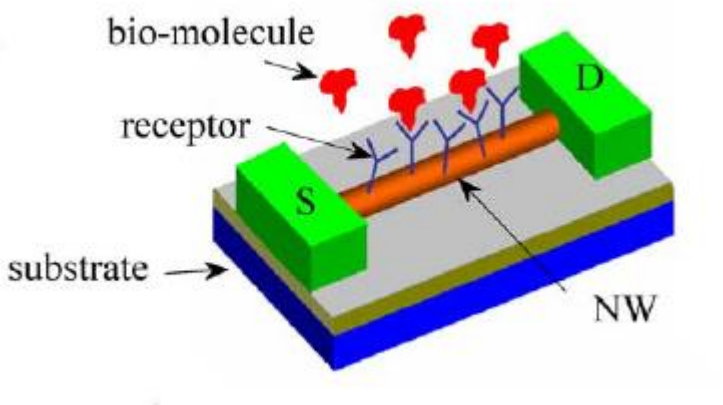

Figure 3.3.1: Schematic of a Si-NW biosensor

A general scheme for detecting biomolecules using Si-NW sensor is shown in Figure 3.3.1. The system consists of a Si-NW between two electrodes. The surface of the nanowire is functionalized with specific receptors that recognize and bind only to the target molecules. The electrodes are protected from the solution by an oxide layer to avoid any undesired conductance change due to modification of electrode work function. When the sensor is immersed in an analyte solution some of the target molecules diffuse through the solution and reach the NW and get captured by the receptors and thereby binding them close to the surface. Many biomolecules carry an electrostatic charge under normal physiological conditions. The Coulomb interaction between the charge of the target biomolecule and the NW can result in a change in conductivity of the latter.

3.4 GROWTH OF Si-NW SENSOR

Several methods have been explored to fabricate nanoscale biosensor based on "bottom-up" approach, are limited by complex integration, requiring transfer and positioning of an individual nanostructure and making reliable ohmic contacts. A study was demonstrated for the detection of DNA molecules based on their intrinsic charge by using silicon nanowires (Si-NWs) fabricated by standard "top-down" approach [16].

Si-based nanoscale sensors with a set of Si-NWs 50 nm wide, 60 nm high and 20 μm long were fabricated using silicon-on-insulator (SOI) wafers. The SOI wafers, which had a 60 nm single-crystal layer on a 200 nm thick SiO_2 insulating layer, were doped by ion implanting with boron or phosphorus to concentrations between $10^{16}cm^{-3}$ and 10^{19} cm^{-3}, followed by activation at 925 °C in a N_2 ambient for 10 min. The top Si layer was then patterned by e-beam lithography.

The Si-NWs and their micron-scale electrical leads were formed on the top of the SiO_2 insulating layers by reactive ion etching (RIE). To decrease the density of surface dangling bonds on the Si surface and increase the stability of the sensors, a thin SiO_2 layer with a thickness of 3 nm was grown on the Si nanowire surfaces by annealing the wafer at 900 °C in an O_2 ambient for 1 min. An aluminum layer of 100 nm thickness was deposited by e-beam evaporation on top of the Si leads after removing the 3 nm SiO_2 layer (using 1:10 HF solution) in these areas to form electrical contact with the Si and reduce the resistance of the electrical leads. The samples were then annealed in forming gas (3.8% hydrogen in nitrogen)

at 450°C for 30 min to make reliable ohmic contact between the aluminum and Si as well as to remove the interface states between the Si-NWs and the thermal oxide. Finally, to eliminate any interference from the electronic leads during sensor tests, the area outside of the Si-NW regions was coated with a 100 nm silicon oxide layer. Thus, only the Si-NWs were exposed to the environment during sensor testing.

Before the surface modification, the surface of the Si-NWs was treated with water-vapor plasma. The plasma treatment cleaned the sample surfaces and generated a hydrophilic surface by hydroxy-terminating the silicon oxide surfaces. A self-assembled monolayer with free thiols on the surface was then prepared using a gas-phase method. The samples were exposed to the vapor of 3-mercaptopropyl-tri-methoxysilane (MPTMS) in argon for 4 h, followed by rinsing with absolute ethyl alcohol, and blowndry with nitrogen. The immobilization of ss-DNA probes was achieved by exposing the MPTMS-covered samples to a 5 μM solution of the oligonucletides modified with acrylic phosphoramidite functional groups at the 5ss position for 12 h. The immobilization of DNA probes was confirmed by attenuated total reflection infrared spectroscopy (ATR-IR) on a silicon ATR crystal. Compared with noncovalent attachment methods, the covalent anchoring of oligonucleotides on the Si-NW surface provided better stability and less nonspecific hybridization for DNA sensing.

3.5 PERFORMANCE PARAMETERS OF Si-NW SENSOR

The response of a biosensor is characterized in terms of its *selectivity*, *settling time*, and *sensitivity* [1].

Selectivity quantifies the ability of a sensor to detect the desired target via “lock-and-key” principle in the presence of a host of almost similar molecules, called parasitic or interfering molecules. Without high degree of Selectivity, one might require extensive sample preparation and prefiltration that would offset the perceived cost advantages of the label-free technology. Therefore, Selectivity of label-free biosensors represents an important optimization problem where theoretical models can play a defining role in reducing the experimental overhead in evaluating technology options [17]. Selectivity of a sensor is entirely determined by the surface functionalization schemes.

The time taken by the sensor to produce a stable signal change defines the *settling time*. It is determined by biomolecule concentration, their diffusion coefficients, and their conjugation affinity to the receptor molecules.

Finally, *sensitivity* corresponds to the relative change in sensor characteristics upon attachment of target molecules on nanowire surface. This is mainly determined by the electrostatics of the system.

3.6 TARGET AND RECEPTOR BIOMOLECULES

Detection of target biomolecules in a solution is a two step process. *The first step* involves functionalization of the sensor surface with receptor molecules specific to the desired target. And the *second step* is the "receptor functionalized sensor" is introduced to a solution containing target biomolecules as well as other parasitic molecules.

3.6.1 FUNCTIONALIZATION OF THE SENSOR SURFACE WITH RECEPTOR BIOMOLECULES

The transformation of a nanowire into a biosensor requires surface functionalization, such that biologically active ligands are conjugated to the sensor surface. Conventional Si-NW biosensors have the ligand attached directly to the SiO_2 sensor surface using silane-based attachment chemistry. In this case, the solution containing the receptor molecules is introduced to the sensor surface. Subsequently these receptor molecules diffuse within the fluidic volume to eventually (and sequentially) attach to the sensor surface at random locations [17]. However, conjugating to the SiO_2 layer reduces the sensor selectivity because the entire substrate surface is most often a homogeneous oxide surface [18]. Selective functionalization to oxide passivated Si-NWs has been reported [19].).

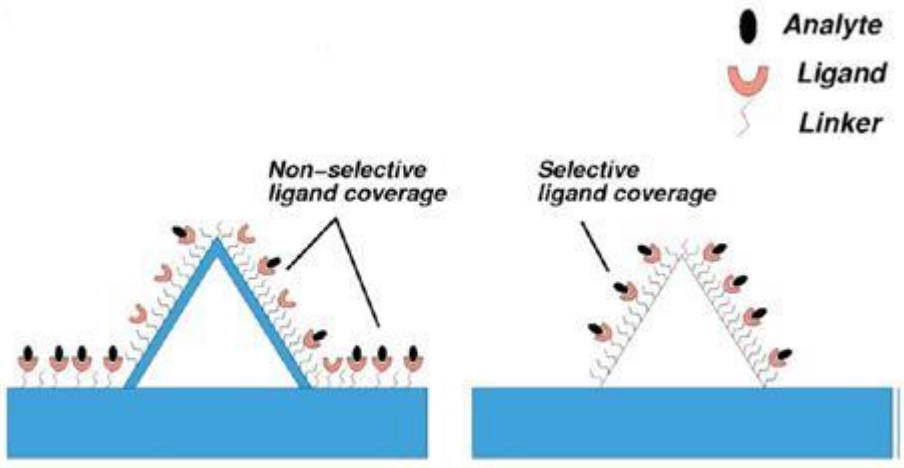

Figure 3.6.1: Conventional homogeneous and Selective heterogeneous functionalization with ligands conjugated to the Si-NW sensor.

Figure 3.6.1 shows a cross-section of a triangular Si-NW with conventional nonselective functionalization as the ligands cover the entire homogeneous surface, which drastically reduces the number of analytes that bind to the sensing surface. Figure 3.6.1 also shows a selectively functionalized Si-NW biosensor where the ligands are conjugated exclusively to the silicon surface and the entire surface is heterogeneously functionalized. Detection sensitivity of ligand-analyte binding is dependent on the distance from the charged analyte to the silicon surface, which includes analyte, ligand, and linker (Figure 3.6.1).

3.6.2 STRUCTURE OF TARGET BIOMOLECULES

Many biomolecules carry an electrostatic charge under normal physiological conditions. For example, DNA is negatively charged, whereas the net charge of a protein molecule depends on the pH of the solution [20]. The net charge of a biomolecule depends on its structure. Among various biomolecules the detection of DNA is of special interest because of its high affinity to conjugate with other receptor biomolecules and with itself as well.

DNA (deoxyribose nucleic acid) is a nucleotide polymer, found primarily in the nucleus of cells. The linear backbone of a DNA molecule consists of alternating sugar residues and

phosphate groups. The bond linking an individual sugar residue to the neighbouring sugar residues is a 3, 5 -phosphodiester bond. This means that a phosphate group links carbon atom 3 of a sugar to carbon atom 5 of the neighbouring sugar (**Figure 3.6.2**)

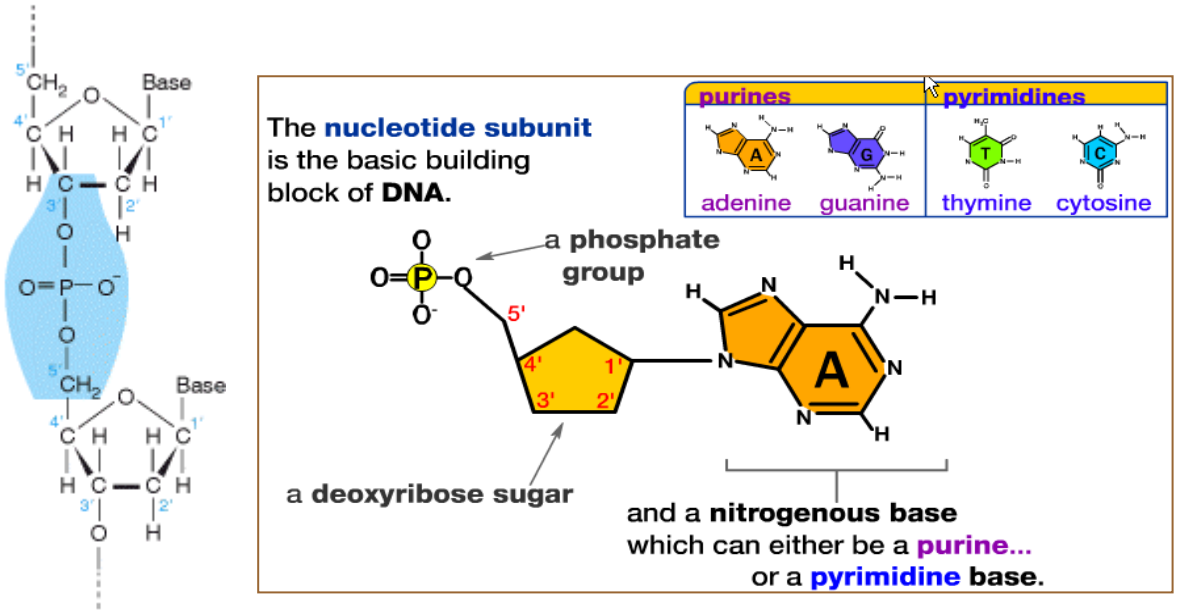

Figure 3.6.2: A 3 -5 phosphodiester bond.

The structure of DNA is a double helix in which two DNA molecules (DNA strands) are held together by weak hydrogen bonds to form a DNA duplex. Hydrogen bonding occurs between laterally opposed bases (base pairs), of the two strands of the DNA duplex according to Watson-Crick rules: adenine (A) specifically binds to thymine (T) and cytosine (C) specifically binds to guanine (G). A-T base pairs have two connecting hydrogen bonds; G-C base pairs have three (Figure 3.6.3)

Adenine bonds only with Thymine

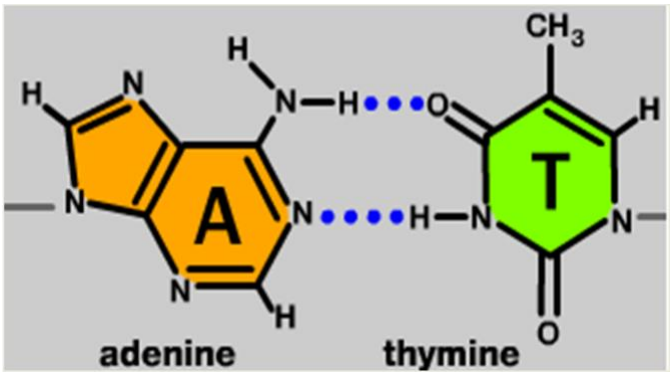

Guanine bonds only with cytosine

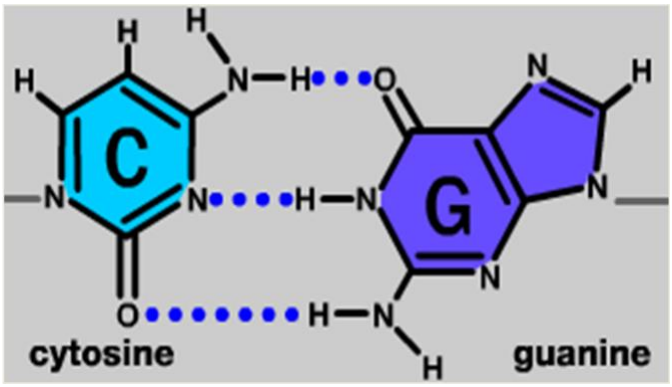

Figure 3.6.3: A-T and C-G base pairs

DNA can adopt different types of helical structure. A-DNA and B-DNA are both righthanded helices (ones in which the helix spirals in a clockwise direction as it moves away from the observer). They have respectively 11 and 10 base pairs per turn. Z-DNA is a left-handed helix which has 12 base pairs per turn. The *pitch* of each helix represents the distance occupied by a single turn and accommodates 12 nucleotides in Z-DNA. The two DNA strands of a DNA duplex are said to have complementary sequences and the sequence of bases of one DNA strand can readily be inferred if the DNA sequence of its complementary strand is already known. . The two strands of a DNA duplex are said to be antiparallel because they always associate in such a way that the 5-3 direction of one DNA strand is the opposite to that of its partner.

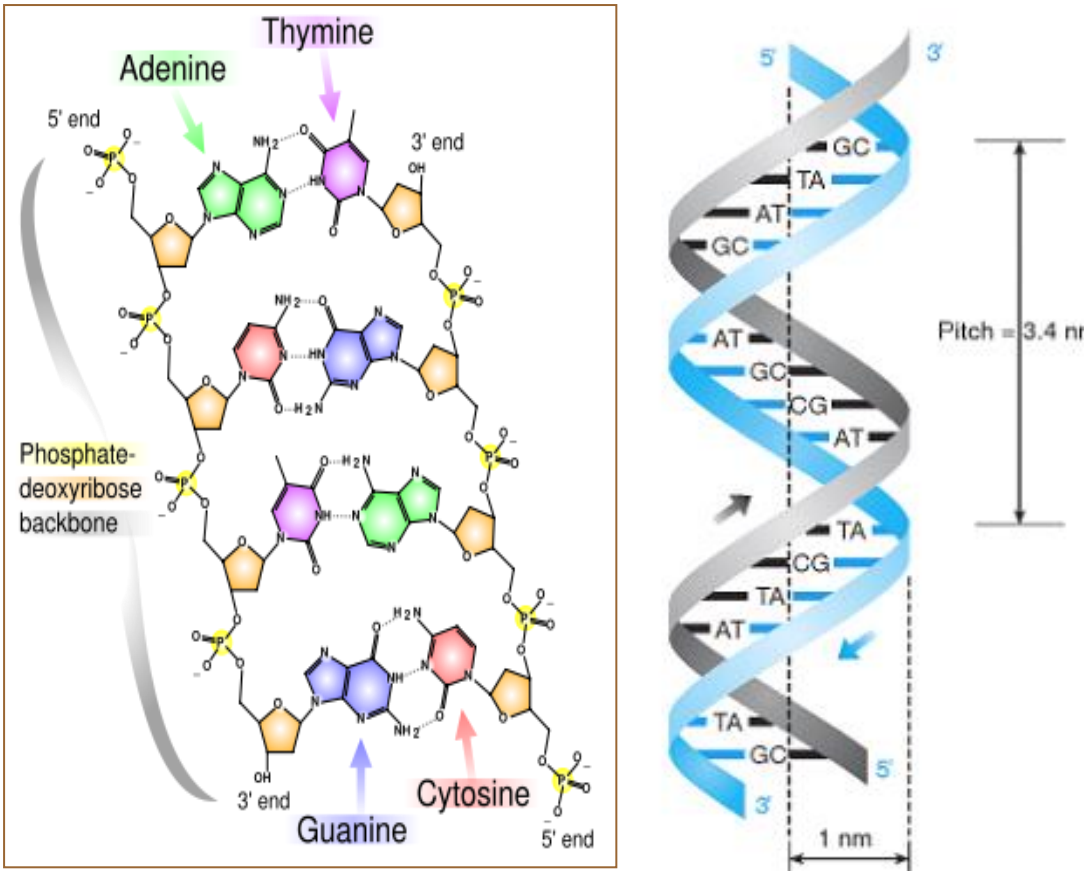

Figure 3.5.3: Double helical structure of DNA molecule

The charge of a DNA arises due to the presence of phosphate ions in the backbone of DNA helix and not due to the individual base pair. Each phosphate has 4 oxygen atoms, two are occupied in phosphodiester bond and rest two is unoccupied and stays in anionic state.

Chapter 4

MODELLING AND SIMULATION METHODS

4.1 DIFFUSION-CAPTURE MODEL

4.1.1 MODEL EQUATIONS

Time dynamics of molecule capture on a sensor surface is essentially a two step process: transport of the target molecules to the sensor surface and the subsequent conjugation with the receptor molecules. The response of a nanoscale sensor depends on the analyte concentration as well as dimensionality of the sensor. Consider an isolated sensor immersed in a static analyte solution at time t=0 (Figure 4.1.1). The surface of the sensor is functionalized with specific receptors for the target molecules. The diffusion of analyte particles towards a planar device (ISFET) is 1D, and towards a cylindrical nanowire surface is 2D. The Diffusion-Capture (D-C) model assumes that the molecule transport is diffusion limited and the target-receptor conjugation is treated as a first-order chemical reaction [21].

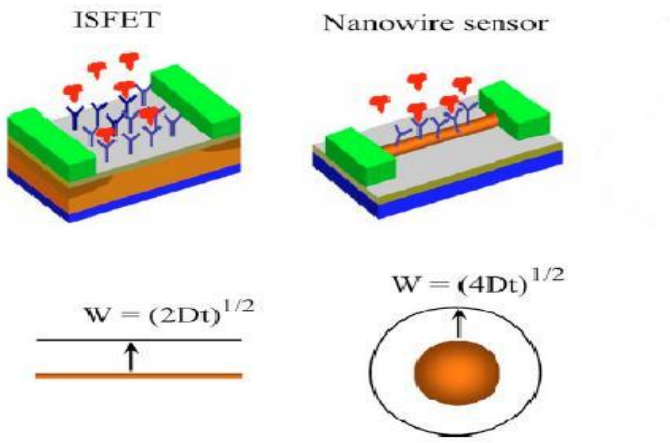

Figure 4.1.1: Schematic of a sensor immersed in analyte solution. Equilibrium analyte concentration is assumed at a distance W from the sensor surface.

The rate of conjugation between the target and the receptors is given by

$$\frac{dN}{dt} = k_F(N_0 - N)\rho_s - k_R N \tag{4.1.1}$$

where N is the density of conjugated receptors, N_0 is the density of receptors on the sensor surface, k_F and k_R are the capture and dissociation constants (forward and reverse reaction coefficients), and ρ_s is the concentration of analyte particles at the sensor surface at any given time t. The first term of equation (4.1.1) represents the conjugation between the target and the receptors while the second term denotes the detachment (due to thermal fluctuation, etc.). ρ_s is determined by the diffusion of target molecules set by the concentration gradient at the sensor surface which is given by

$$\frac{d\rho}{dt} = D\nabla^2\rho \tag{4.1.2}$$

where D is the diffusion coefficient of target molecules in the solution that depends on the fluidic environment and size of the target biomolecule. Equation 4.1.1 and 4.1.2 are numerically solved to get the transient response of biosensors.

4.1.2 ANALYTICAL SOLUTION OF D-C EQUATIONS

The time response of the sensors as well as the relationship among various sensor parameters is obtained by solving equation 4.1.1 and 4.1.2 simultaneously. An approximation to exact solution can be derived by generalizing the approach by Berg [21]. For large k_F/k_R ratio and large receptor density (N_0) equation 4.1.1 may be simplified as:

$$\frac{dN}{dt} \approx k_F N_0 \rho_s \tag{4.1.3}$$

The solution of Equation 4.1.2 *in any dimension at steady state* is given by [17]:

$$I = JA_D = C_{D,SS}(\rho_0 - \rho_s) \tag{4.1.4}$$

where I is the integrated incident flux to the sensor, A_D is the dimension-dependent area of the sensor surface, ρ_0 is the equilibrium analyte concentration at a distance W from the sensor surface and $C_{D,SS}$ is the diffusion equivalent capacitance. For one dimensional diffusion $C_{D,SS} = D/W$ and for two dimensional diffusion it is given as:

$$C_{D,SS} = \frac{2\pi D}{\log\left[(W+a_0)/a_0\right]} \tag{4.1.5}$$

At steady state, the incident flux must balance the conjugation flux, so that $J = dN/dt$. Then equation 4.1.3 and 4.1.4 can be solved to calculate steady state flux to the sensor surface, i.e.,

$$k_F N_0 \rho_s A_D = C_{D,SS}(\rho_0 - \rho_s)$$

or,

$$k_F N_0 \rho_s \left(\frac{A_D}{C_{D,SS}} + \frac{1}{k_F N_0}\right) = \rho_0$$

or,

$$\frac{dN}{dt} = \rho_0 \left(\frac{A_D}{C_{D,SS}} + \frac{1}{k_F N_0}\right)^{-1}$$

or finally,

$$N(t) = \rho_0 t \left(\frac{A_D}{C_{D,SS}} + \frac{1}{k_F N_0}\right)^{-1} \tag{4.1.6}$$

4.1.3 APPLICATION OF D-C MODEL

4.1.3.1 EVALUATING TRANSIENT RESPONSE

It can be easily realized that as the forward reaction progresses, the analyte near the sensor surface is depleted as more molecules diffuse to the sensor surface and are captured by the surface receptors. Then a new diffusion equivalent capacitance, $C_D(t)$ can be defined which is a function of the depletion distance, $W(t) = \sqrt{2nDt}$, where n is dimensionality of the sensor.

For planar ISFET sensor n=1 and

$$C_D(t) = \frac{D}{\sqrt{2Dt}} \tag{4.1.7}$$

And for cylindrical Si-NW sensor n=2 and

$$C_D(t) = \frac{2\pi D}{\log\left(\frac{\sqrt{4Dt}+a_0}{a_0}\right)} \tag{4.1.8}$$

Then the transient response for a planar ISFET sensor is given by,

$$N(t) = \rho_0 t \left(\frac{\sqrt{2Dt}}{D} + \frac{1}{k_F N_0}\right)^{-1} \tag{4.1.9}$$

And response for a cylindrical Si-NW sensor is:

$$N(t) = \rho_0 t \left(\frac{a_0 \log\left(\frac{\sqrt{4Dt}+a_0}{a_0}\right)}{D} + \frac{1}{k_F N_0}\right)^{-1} \tag{4.1.10}$$

4.1.3.2 ESTIMATING MINIMUM DETECTABLE CONCENTRATION

Define the number of analyte particles required to capture for minimum amount of detectable signal change as N_s. Then the time required to capture N_s particle is defined as settling time (t_s). Then approximating 1/ ($k_F N_0$) ≈ 0 the settling time for planar ISFET and cylindrical Si-NW sensors can be calculated from equation 4.1.9 and 4.1.10 respectively.

For planar ISFET sensor settling time (t_s) is derived as a function of analyte concentration (ρ_0):

$$N_s \approx \rho_0 t_s \frac{D}{\sqrt{2Dt_s}}$$

or,

$$t_s \cong \frac{2N_s^2}{D\rho_0^2} \tag{4.1.11}$$

For cylindrical Si-NW sensor (two dimensional diffusion of analyte biomolecule) settling time (t_s) can be derived as:

$$t_s \cong \frac{N_s a_0 \log\left[(\sqrt{4Dt_s}+a_0)/a_0\right]}{\rho_0 D} \tag{4.1.12}$$

The minimum detectable concentrations for planar ISFET and cylindrical Si-NW sensor can be determined by calculating response time t_s using equation 4.1.11 and 4.1.12.

4.2 POISSION-BOLTZMANN EQUATION

4.2.1 MODEL BASED ON PB EQUATION

Consider a Si-NW sensor is immersed in an electrolyte solution whose surface is functionalized with specific receptor (Figure4.2.1a). Figure 4.2.1b shows a Cross-section of the sensor along the dotted line shown in (4.1a). The system can be divided into three subregions, as shown in Fig. 4.2.1b (1) cylindrical Si-NW of diameter *d*; (2) insulating native oxide around the NW of thickness t_{OX}; and (3) electrolyte that contains the target

biomolecules, and the various ions that provide the necessary buffer for the stability of target–receptor binding.

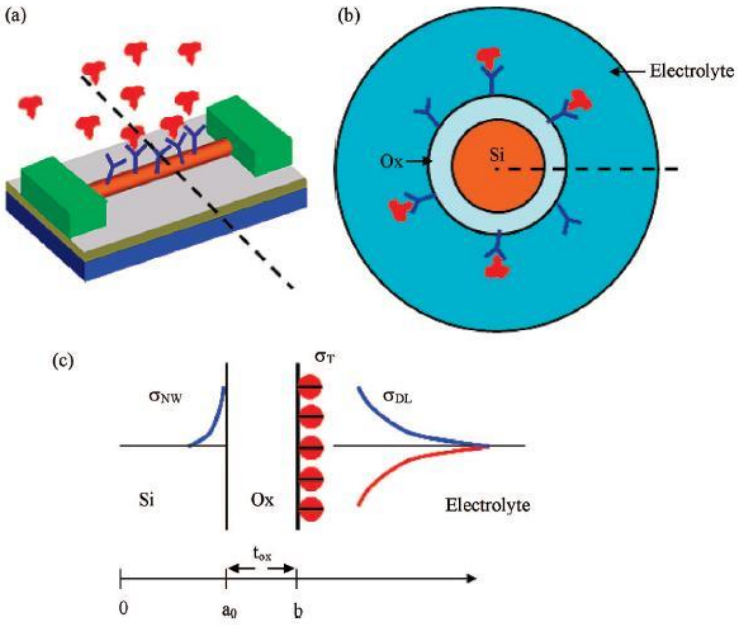

Figure 4.2.1: Schematic of Si-NW biosensor. (a) NW surface is functionalized with receptors for target biomolecules. (b) Cross-section of the sensor along the dotted line shown in (a). (c) Charge distribution in the sensor system along the dotted line shown in (b).

In region 1 conductance modulation is due to fixed charge of biomolecules (the DNA molecule has a set of fixed negative charges due to the phosphate backbone of the DNA chain). The fixed charges can be modeled using delta function:

$$\sigma_{fixed} = q \sum_{i=1}^{N} Z_i \delta(r - r_i) \tag{4.2.1}$$

where q is the elementary charge (q=1.6×10^{-19}C), N is the number of fixed charges present, Z_i and r_i are their partial charges and positions, and $\delta(r)$ is the Dirac delta function.

Gauss's law relates the electric charge distribution to the resulting electric field. The differential form of Gauss' law [APPENDIX A] for a linear dielectric can be written as:

$$-\nabla.(\varepsilon \nabla \varphi) = \sigma \tag{4.2.2}$$

Then the Gauss' law in region 1 can be written as:

$$-\nabla.(\varepsilon_{Si}\varphi(r)) = q\sum_i^N Z_i\delta(r-r_i) \tag{4.2.3}$$

In region 2, the charge density function equals to zero due to the absence of mobile ions in the oxide layer. The Gauss' law in region 2 becomes:

$$-\nabla.(\varepsilon_{ox}\nabla\varphi(r)) = 0 \tag{4.2.4}$$

In region 3, the charge distribution is due to the mobile ions in the solution. The distribution of mobile charges can be described using Boltzmann distribution [APPENDIX B]:

$$\sigma_{mobile} = \sum_j^{N_{ions}} qZ_j I_0 N_{avo} exp(\frac{-qZ_j\varphi(r)}{k_B T}) \tag{4.2.5}$$

where N_{ions} is the number of the mobile ions, $Z_j$is the charge of the ion, I_0 is the concentration of the ion, N_{avo} is the Avogadro number, k_B is the Boltzmann constant, T is the temperature and Φ is the electrical potential.

Then using equation 4.2.2:

$$\nabla.(\varepsilon_w\nabla\varphi(r)) = -\sum_j^{N_{ions}} qZ_j I_0 N_{avo} exp(\frac{-qZ_j\varphi(r)}{k_B T}) \tag{4.2.6}$$

By defining piecewise dielectric constant function ε(r) and a parameter Ω(r) as:

$$\varepsilon(r) = \begin{cases} \varepsilon_{Si} & for\ region\ 1 \\ \varepsilon_{OX} & for\ region\ 2 \\ \varepsilon_{w} & for\ region\ 3 \end{cases} \tag{4.2.7}$$

$$\alpha(r) = \begin{cases} 0, & for\ region\ 1\ and\ 2 \\ 1, & for\ region\ 3 \end{cases}$$

a single equation can then be written governing the electrostatic potential in all the three regions:

$$\nabla.(\varepsilon(r)\nabla\varphi(r)) = -q\sum_i^N Z_i\delta(r-r_i) - \alpha(r)\sum_j^{N_{ions}} qZ_jI_0N_{avo}exp(\frac{-qZ_j\varphi(r)}{k_BT}) \tag{4.2.8}$$

The above equation can be reduced to a nonlinear elliptic partial differential equation known as nonlinear Poisson-Boltzmann equation [33]:

$$-\nabla.\left(\varepsilon(r)\nabla\varphi(r)\right) + 2\,\alpha(r)qI_0N_{avo}\sinh(\frac{q\varphi(r)}{k_BT}) = q\sum_i^N Z_i\delta(r-r_i) \tag{4.2.9}$$

For region 3 this equation can be rewritten as:

$$-\nabla^2\varphi(r) + \frac{k^2}{\beta}\sinh(\beta\varphi(r)) = \frac{q}{\varepsilon_w}\sum_i^N Z_i\delta(r-r_i) \tag{4.2.10}$$

where,

$$k^2 = \frac{2q^2I_0N_{avo}}{\varepsilon_w k_BT} \tag{4.2.11}$$

and

$$\beta = \frac{q}{k_BT} \tag{4.2.12}$$

k_B is the Boltzmann constant, T is the temperature, and q is the electronic charge(1.6×10^{-19}C), ε is the dielectric constant, and the subscript w represents electrolyte. I_0 is the ion concentration in molar units, and N_{avo} is the Avogadro's constant, whereas the sinh term denotes the contribution due to a 1–1 electrolyte (e.g., Na+ − Cl−), whose ions are assumed to follow Boltzmann distribution (Appendix A). The right-hand side denotes the fixed charge due to the biomolecule, Z_i and r_i denoting the partial charge and location of the atoms within the biomolecule, respectively. k is the Debye- Hückel screening parameter. k^{-1} is called the Debye screening length, it is an important parameter to characterize the thickness of the ion atmosphere, which is an electrical double layer.

4.2.2 ANALYTICAL SOLUTION OF PB EQUATION

Figure 4.2c depicts the charge distribution in the sensor system. If ion concentration in the electrolyte is zero **($I_0 = 0$),** the charge density (σ_T) due to analyte molecules on the sensor surface is equal to the charge induced in the sensor (σ_{NW}).

$$\sigma_T = -\sigma_{NW} \tag{4.2.13}$$

The charge density due to analyte biomolecules is given by

$$\sigma_T \cong \sigma_S N(t) \tag{4.2.14}$$

where σ_S is the charge of a biomolecule. Note that σ_T has been approximated by the charge due to captured biomolecules only. This approximation applies to high-sensitivity, low analyte density sensors relevant for modern biosensing applications, where the average analyte molecule spacing is much larger than the Debye-screening length of an electrolyte.

The induced charge density of a heavily doped cylindrical NW can be calculated by using the formula for capacitance of oxide dielectric on cylindrical NW as:

$$\sigma_{NW} = -\frac{\varepsilon_{OX}}{(a_0+t_{OX})\log(1+\frac{t_{OX}}{a_0})}\,\varphi_0 \tag{4.2.15}$$

Where φ_0 is the surface potential, a_0 is the nanowire radius and t_{OX} is the thickness of the oxide layer. From equation 4.2.14 and 4.2.15 the electrostatic potential is found as:

$$\varphi_0 = \frac{\sigma_S N(t)(a_0+t_{OX}) \log(1+\frac{t_{OX}}{a_0})}{\varepsilon_{OX}} \tag{4.2.16}$$

The sensitivity S of a Si-NW sensor is defined as the relative change in conductance:

$$S = \frac{|G-G_0|}{G_0} = \frac{\nabla G}{G_0} \tag{4.2.17}$$

The conductance of a cylindrical Si-NW of radius a_0, uniform continuous doping density N_D, and length L_{NW} is given by

$$G_0 = \frac{q\mu N_D \pi a_0^2}{L_{NW}} \tag{4.2.18}$$

where μ is the mobility of the carriers. If the molecule conjugation on the surface is approximated by a constant surface density σ_{NW} (in charge per square centimeter), then the change in conductance is given by

$$\nabla G = \frac{2\pi a_0 \mu \sigma_{NW}}{L_{NW}} \tag{4.2.19}$$

The sensitivity S is therefore

$$S = \frac{2\sigma_{NW}}{q a_0 N_D} \tag{4.2.20}$$

Equation 4.2.15 and 4.2.20 yields

$$S = \frac{2\varepsilon_{OX}\varphi_0}{qa_0^2 N_D \log(1+\frac{t_{OX}}{a_0})} \tag{4.2.21}$$

Finally the sensitivity is found by combining equation 4.2.21 and 4.2.16

$$S = \frac{2\sigma_S N(t)(a_0+t_{OX})}{qa_0^2 N_D} \tag{4.2.22}$$

Equation 4.2.22 suggests that sensitivity *S* increases with smaller diameter and reduced doping density. This monotonic increase of sensitivity with diameter (or equivalently, surface area of the sensor) has recently been experimentally confirmed [22]. Also it is obvious from 4.2.19 that the relative sensitivity significantly increases on reducing NW length.

The full charge of the captured biomolecules is not effective in modulating the conductance of sensors due to the electrostatic screening of ions present in the electrolyte. To account for screening, one must solve the nonlinear Poisson–Boltzmann equation (4.2.10). The conductance modulation of a NW sensor can be derived from a simple capacitor model shown in Figure 4.2.1c. Applying the Charge conservation rule to the system

$$\sigma_T = -(\sigma_{DL} + \sigma_{NW}) \tag{4.2.23}$$

where σ_{DL} is the net charge in the electrical double layer formed at the sensor surface (which represents the screening due to the ions in the electrolyte).

Analytical solution of equation 4.2.10 in cylindrical coordinates in an infinite medium gives the double layer charge densityσ_{DL}, in terms of the potential at the sensor surface φ_0[16], given by,

$$\sigma_{DL} = -\frac{2\varepsilon_w k}{\beta}\sinh(\frac{\beta\varphi_0}{2})\sqrt{1+\frac{\gamma^{-2}-1}{cosh^2(\frac{\beta\varphi_0}{2})}} \tag{4.2.24}$$

where, $$\gamma = \frac{K_0(kb)}{K_1(kb)}$$

K_n is the modified Bessel function of the second kind of order n and $b = a_0 + t_{OX}$

Equation 4.2.24 shows that charge contribution of the electrolyte increases exponentially with the surface potential and this electrolyte screening reduces the electrical response of nanobiosensors.

Combining equation 4.2.14, 4.2.15, 4.2.23 and 4.2.24 yields

$$\frac{\varepsilon_{OX}}{(a_0+t_{OX})\log\left(1+\frac{t_{OX}}{a_0}\right)}\varphi_0 + \frac{2\varepsilon_w k}{\beta}\sinh\left(\frac{\beta\varphi_0}{2}\right)\sqrt{1+\frac{\gamma^{-2}-1}{cosh^2\left(\frac{\beta\varphi_0}{2}\right)}} = \sigma_S N(t) \tag{4.2.25}$$

Equation 4.2.25 represents the charge conservation of the system. Screening limited kinetic response of nanobiosensors may be obtained by solving equation 4.2.21 and 4.2.25 numerically.

4.2.3 APPLICATION OF PB BASED MODEL

4.2.3.1 STEADY STATE RESPONSE WITH VARIOUS ANALYTE AND ELECTROLYTE CONCENTRATION

At equilibrium the concentration of conjugated biomolecule is found from equation 4.1.6 as:

$$N_{equi} = \frac{k_F N_0 \rho_0}{k_F \rho_0 + k_R} \tag{4.2.26}$$

The steady-state response can be obtained by replacing $N(t)$ in the right-hand side of equation 4.2.25 with N_{equi}. At low analyte concentrations (i.e.,$k_F\rho_0 \ll k_R$), N_{equi} can be approximated as $N_{equi} = (k_F/k_R)N_0\rho_0$ and φ_0 due to highly charged biomolecules like DNA satisfy the relation $\varphi_0 > 1/\beta$. Under these conditions, an approximate solution for φ_0

can be obtained by neglecting the first term of equation 4.2.25 and using the limits $\lim_{x\to\infty} \sinh(x) = e^x/2 = \lim_{x\to\infty} \cosh(x)$. Then equation 4.2.25 leads to:

$$\frac{\varepsilon_w\, k \exp\left(\frac{\beta\varphi_0}{2}\right)}{\beta} \approx \sigma_s N_{equi} = \frac{\sigma_s k_F N_0 \rho_0}{k_R}$$

or equivalently

$$\varphi_0 = \frac{2}{\beta}\left[\ln(\rho_0) - \frac{\ln(I_0)}{2} + C_2\right] \tag{4.2.27}$$

where $C_2 = \ln\left[\frac{\sigma_s k_F N_0}{k_R}\sqrt{\frac{\beta}{2\varepsilon_w q N_{avo}}}\right]$

Now inserting φ_0 into equation 4.2.21 gives the sensor response

$$S = C_1\left[\ln(\rho_0) - \frac{\ln(I_0)}{2} + C_2\right] \tag{4.2.28}$$

where $C_1 = \frac{4\varepsilon_{OX}}{\beta q a_0^2 N_D \log\left(1+\frac{t_{ox}}{a_0}\right)}$

4.2.3.2 STEADY STATE RESPONSE DUE TO pH OF ANALYTE SOLUTION

The net charge density (charge density due to analyte molecules) on the NW surface can be obtained based on first-order chemical kinetics of bond dissociation for the particular type of surface functionalization schemes used (-OH, -NH_2, etc.). The net charge density (σ_{pH}) on the sensor surface is given as [23]:

$$\sigma_{pH} = qN_F \exp\left(\varphi_0 + 2.303(pH - pKa)\right) \tag{4.2.29}$$

where $pKa = -\log_{10} K_a$; K_a is the dissociation constant and N_F is the density of surface functionalization groups.

Then by replacing $\sigma_S N(t)$ (right-hand side of equation 4.2.25) by σ_{pH} and repeating the derivation from section 4.2.3.1 an approximate solution of φ_0 can be obtained as:

$$\varphi_0 = \frac{2}{\beta}[\mathrm{C}_3 + \frac{\ln(I_0)}{2} - 2.303(pH - pKa)] \quad (4.2.30)$$

where $C_3 = \frac{1}{2}\ln(\frac{2\varepsilon_w N_{avo}}{q\beta N_F^2})$

Now inserting φ_0 into equation 4.2.21 gives the sensor response

$$S = C_1[\mathrm{C}_3 + \frac{\ln(I_0)}{2} - 2.303(pH - pKa)] \quad (4.2.31)$$

Equation 4.2.31 predicts the linear dependency of the sensor response to fluctuations in pH of the solution.

4.3 SIMULATION METHODS

The model developed in this thesis is based on Diffusion-Capture equations and non-linear Poisson-Boltzmann equation. Finding efficient solvers to numerically solve the Poisson-Boltzmann equation for a large class of macromolecules has been an active area of research for over a decade. In the current numerical methods, the biomolecular-solvent system is modeled by dielectrically distinct regions with singular charges distributed in the molecular region (fixed point charges in Poisson-Boltzmann equation). The biomolecular-solvent system is then discretized and represented as a distribution of points and their connections. The generation of this presentation, called mesh generation, is generally a difficult task since it is always complicated by the identification of the irregular molecular surface and an appropriate description of this surface for resolving the molecular structure in sufficient details. The fineness of the mesh is critical to the efficiency and accuracy of the numerical methods. A coarser mesh results in higher efficiency but lower accuracy, and vice versa. Once the molecular surface is identified and discretized, the remaining procedure depends on the particular numerical method adopted.

Finite difference method, boundary element method, and finite element method are among the most popular numerical methods. Finite difference method has been the most popular numerical method for solving the Poisson-Boltzmann equation. The major disadvantages in applying the finite difference method to numerically solve the Poisson-Boltzmann equation are the large number of unknowns and the low efficiency of linear solvers in general [24].

In this thesis a simulation tool named BioSensorLab [25] is used for the numerical simulation of Diffusion-Capture equations (4.1.1 and 4.1.2) and nonlinear Poisson-Boltzmann equation (4.2.10). BioSensorLab is a numerical simulator to predict the performance metrics for various types of label-free, electronic biosensors. For solving D-C equations the tool assumes that the molecule transport is diffusion limited and the target-receptor conjugation as a first order chemical reaction. To account for the electrostatic screening BioSensorLab solves nonlinear Poisson-Boltzmann equation (4.2.10) numerically which uses Newton–Raphson iteration for convergence. For the numerical solution of 4.2.10 the tool approximates the NW as an equipotential surface in the electrolyte [essentially as a conducting cylinder] computes the flux on NW surface, and then uses this electric flux as the boundary condition. This simulator ensures correct carrier modulation in NW and gives good estimates for sensitivity.

BioSensorLab needs the following parameters to calculate the electrostatic potential in electrolyte: the dimension information of various layers and electrolyte, the doping density of the Si-NW, the ion concentration of the electrolyte, the interface charge density and the diffusion coefficient in the electrolyte solution. The dimension information of various layers is chosen using the considerations that channel length of Si-NWs used for biomolecule detection (2–20 μm), is much larger than the mean free path of electrons in silicon (of the order of 10 nm) and the radius of the nanowire is chosen such that the design is feasible in practical implementation. The interface charge density can be calculated using the dimension information and the net charge of biomolecule conjugation. The structure of the biomolecule is obtained from the Protein Data Bank (PDB) [26]. The charge distribution of these biomolecules can be mapped from the force field parameters of Molecular Dynamics simulators (GROMACS [27]).

This thesis involves the simulation study to investigate the sensor performance. Both the D-C equations and Poisson-Boltzmann equation are solved analytically and simulation is carried out using MATLAB program. For this simulation process it is more crucial to calculate the net charge of the biomolecule conjugate (DNA). Since the base pairs contribute zero charge [20], only the backbone of the DNA strands is considered. DNA strands are negatively charged due to the presence of phosphate ions in their backbone. Charge of a DNA molecule does not depend on the pH of the solution. Getting the molecule structure from Protein Data Bank (PDB) the net charge is calculated using the Molecular Dynamics simulators (GROMACS). The model developed in this thesis is diffusion limited and another important parameter for this simulation study is the diffusion coefficient. In aqueous solutions, diffusion coefficients of the DNA fragments in water, D(w) decreased from 53×10^{-8} to 0.81×10^{-8} cm^2/s for sizes of 21-6000 bp. Diffusion coefficients of the DNA, D is related empirically to DNA size: $D= 4.9 \times 10^{-6}/ .[bp]^{(0.72)}$ cm^2 /s [39].

The simulation process described above is then implemented in MATLAB program. When the calculation process is written in MATLAB program obviously it needs more steps such as declaration of physical constants and input variables.

Chapter 5

RESULTS AND DISCUSSION

5.1 INTRODUCTION

The design of a nanoscale biosensor greatly depends on the dimension of the nanostructures, their doping density and also the parameters (analyte concentration, ion concentration, pH of the solution, etc.) related to the sensor application environment that seriously affect the sensor performance. The response of a sensor is characterized in terms of its settling time, sensitivity and selectivity. In this thesis performance is measured by calculating the settling time and sensitivity only. The parameter selectivity involves the statistical properties of biomolecule adsorption and is left for the extension of this work. Although analytical solution of the model based on diffusion capture equations and Poisson-Boltzmann equation provide a rough theoretical estimate for the performance parameters of nanobiosensors, the implications of this model are actually profound and it gives one a very sophisticated understanding of electronic biosensing.

In this thesis first settling time is calculated for both planar ISFET and cylindrical Si-NW sensors and compared. Then the transient capture of target molecules on the sensor surface is analyzed without taking into account for the screening by electrolyte solution, and responses for ISFET sensor and Si-NW sensor are compared. Finally sensitivity of the Si-NW sensor is studied to show how electrostatic screening affects the sensor performance. All the analytical results are checked against exact numerical results found from BioSensorLab, a numerical simulator.

5.2 RESULTS AND ANALYSIS

The most attractive feature of nanoscale biosensor is that its performance improves as the diameter of the nanowire as well as doping density decreases. Figure 5.2.1 shows the sensitivity of Si-NW sensor increases as radius of the NW decreases for varying doping density. This is well established and the graph reproduced here to account for the significance of biosensors in nanoscale.

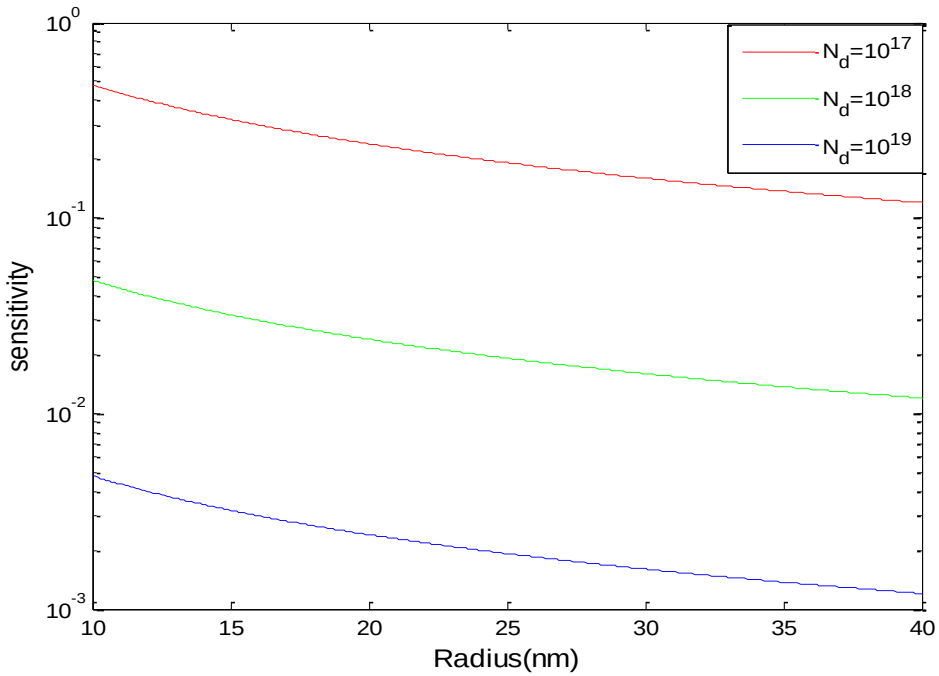

Figure 5.2.1: Sensitivity of NW sensor as function of radius.

Sensitivity for three different doping levels ($N_d=10^{17}cm^{-3}$, $10^{18}cm^{-3}$ and $10^{19}cm^{-3}$) is investigated. Nanowire length is kept constant (2µm) and air is assumed as the surrounding medium of the nanowire. Figure 5.2.1 clearly shows that sensitivity increases with smaller diameter and reduced doping density, which is consistent with equation 4.2.22. Also the relative sensitivity significantly increases on reducing NW length particularly for higher doping densities. This is reasonable since for shorter Si-NW the travelling speed of carriers is faster. But apart from the technological difficulties associated with the continued scaling of dimensions, doping also cannot be reduced to low values without introducing significant variation in sensor performance.

Figure 5.2.2 shows the sensor response time as function of analyte concentration for both planar ISFET sensor (green) and cylindrical NW sensor (red). The results are obtained for a typical DNA detection problem. In aqueous solutions, diffusion coefficients of the DNA fragments is related empirically to DNA size: $D= 4.9 \times 10^{-6}[\text{bp size}]^{(-0.72)}$ cm^2/s. In this study, response time is calculated for bp size 12. The minimum number of analyte particles required for the minimum amount of detectable signal is taken as 10 (μm^{-2}). The sensor dimension is selected as: both length and width of ISFET sensor and radius of the NW are taken 30 cm. The thickness of the oxide layer is taken as 1nm.

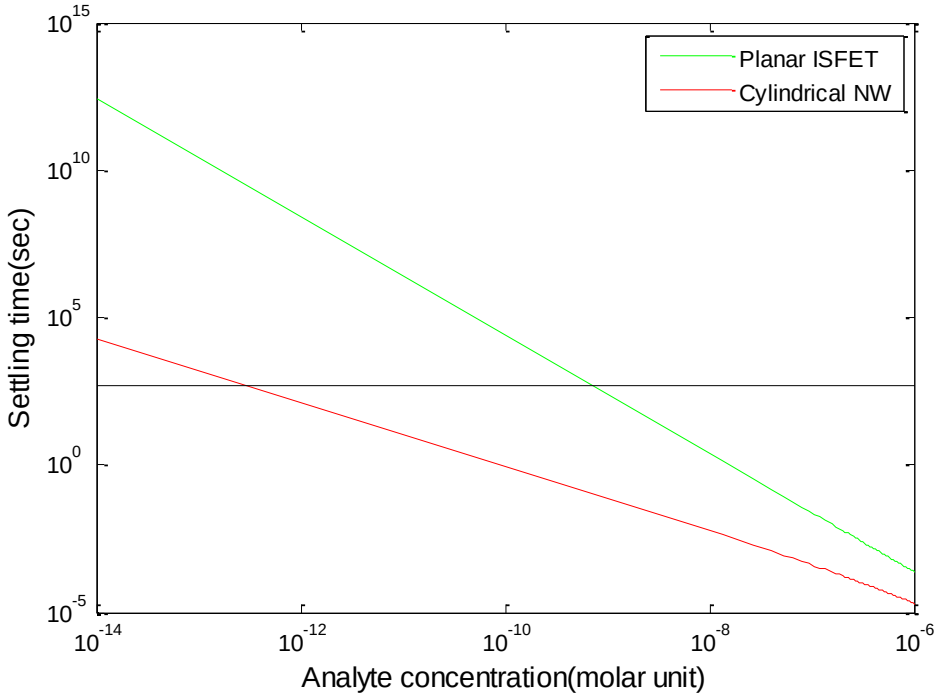

Figure 5.2.2: Response time for Si-NW (red) and ISFET (green) sensor as function of analyte concentration (analytical simulation).

Figure 5.2.2 allows one to predict the trade-off between settling time and the minimum detectable concentration for planar (1D) and cylindrical (2D) nanosensors for a typical DNA detection problem. For a reasonable incubation time (500 sec), a 2D cylindrical Si-NW sensor can detect down to about 300 fM concentrations whereas a 1D planar sensor based on ISFET can detect only to nanomolar levels. Thus there exist fundamental limits in the concentration of biomolecules which can be detected by any sensor under reasonable settling time. And the detection limit of a typical 2D nanowire sensor (for the same response time) is three to four orders of magnitude higher compared to planar 1D sensor. Then with proper

design and technology development, Si-NW -based cylindrical sensors should be able to achieve ultrafast detection (~500 sec) at femtomolar concentration.

Equation 4.1.11, equation 4.1.12 and Figure 5.2.2 combindly provide specific guidance for design of more sensitive nanobiosensor. This may be achieved by reducing the diameter of the sensor, decreasing the minimum number of analytes required for detectable signals and increasing the effective diffusion coefficient *D* by increasing the ambient solution temperature without exceeding the melting point of the target-analyte conjugate.

Finally, once a sensor has been calibrated for a biomolecule of known diffusion coefficient, Equation 4.1.12 can be used for electrical determination of diffusion constants of unknown biomolecules based on the geometry of the sensor and the average response time

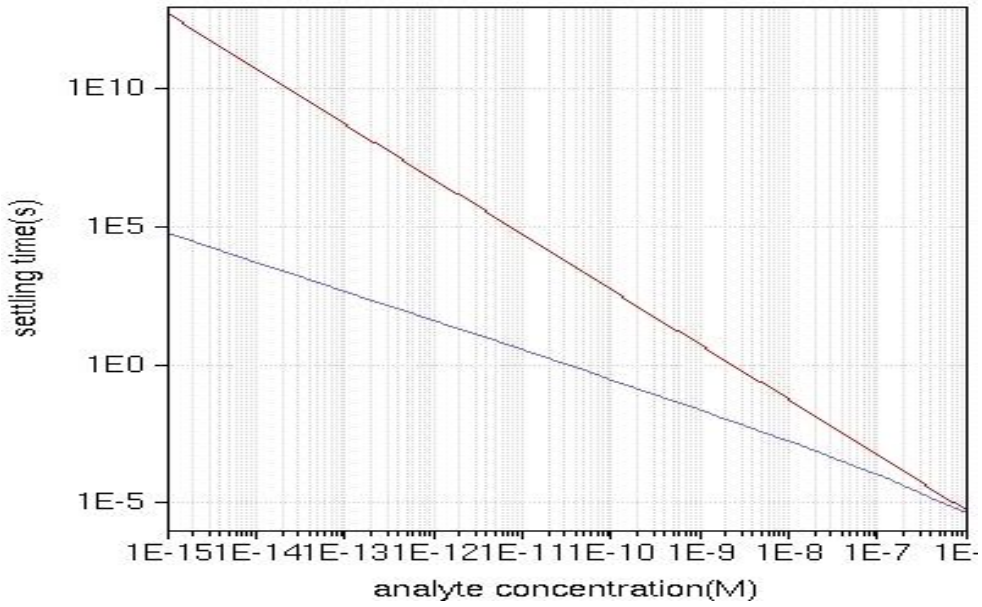

Figure 5.2.3: Response time for Si-NW (blue) and ISFET (red) sensor as function of analyte concentration (numerical simulation).

Figure 5.2.3 presents the numerical results (response time versus analyte concentration) for both Si-NW and ISFET sensors. The results are obtained by numerically solving the equations 4.1.1 and 4.1.2 using the simulation tool BioSensorLab. This numerical result strongly support the results obtained from analytical simulation using MATLAB.

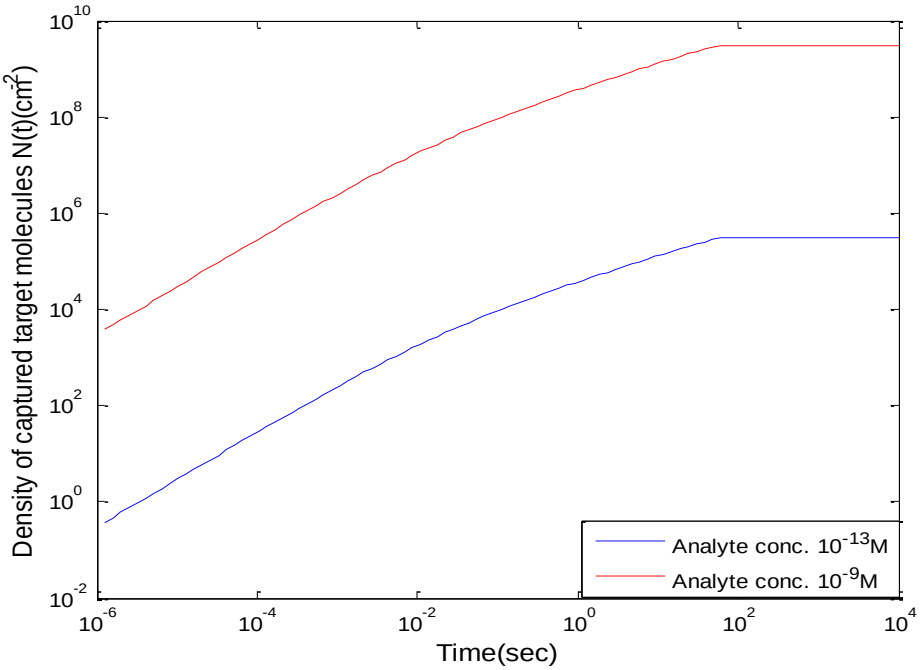

Figure 5.2.4: Transient response for planar ISFET sensor (density of captured target molecules vs time)

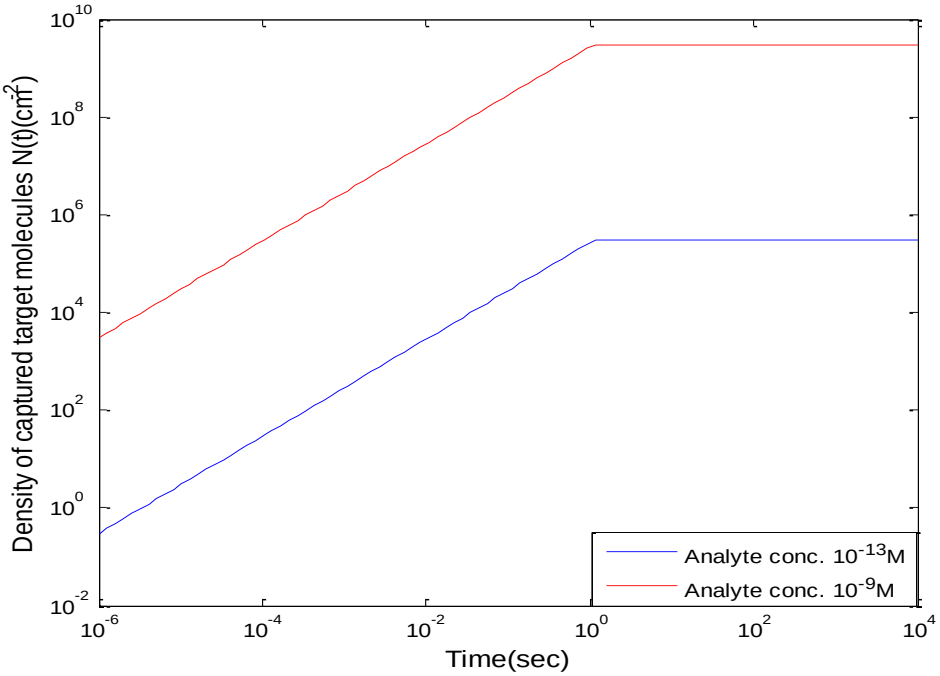

Figure 5.2.5: Transient response for cylindrical Si-NW sensor (density of captured target molecules vs time)

Figure 5.2.4 and 5.2.5 shows the transient response of planar ISFET and cylindrical Si-NW biosensor. Two curves (blue and red) show sensor response at two different analyte concentrations (100 fM and 1 nM). As can be seen sensor response improves as time goes and become saturated after a certain time. This saturation is due to the balance of forward and backward reaction. It is seen that the number of captured analyte molecules increases with analyte concentration as expected.

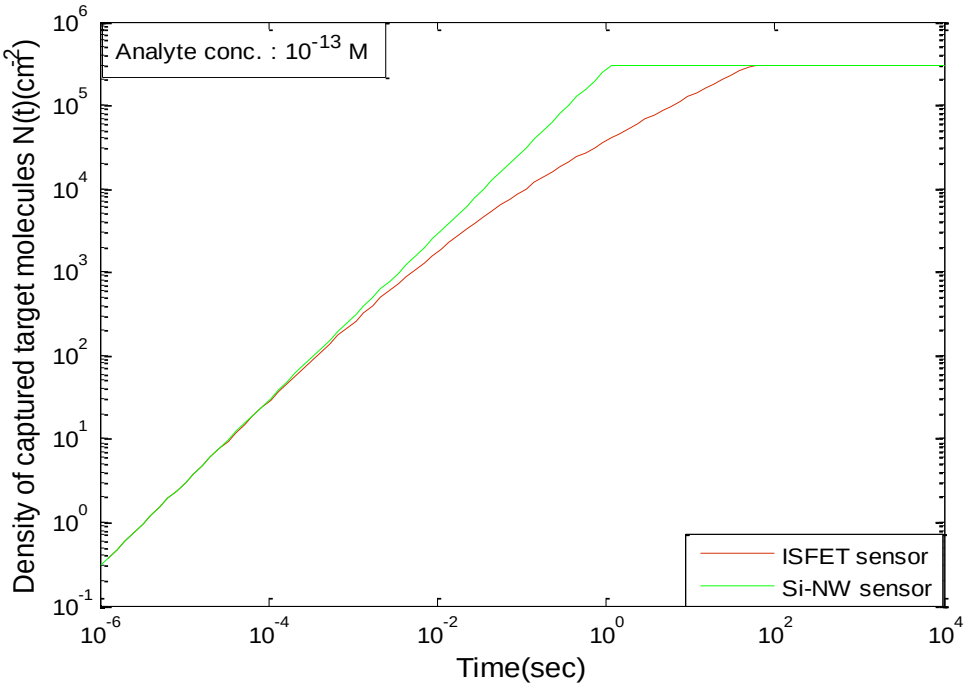

Figure 5.2.6: Comparison of sensor response between ISFET and Si-NW sensor at 100 fM analyte concentration (analytical simulation).

Figure 5.2.6 allows one to make a comparison for biomolecule conjugation between planar 1D and cylindrical 2D nanosensors. It is seen that the conjugation of target biomolecules for Si-NW sensor reach equilibrium fast than that of ISFET sensor. Hence the 2D Si-NW sensor gives faster response. Also it can be seen that at first sensor response varies linearly with time both for ISFET and Si-NW sensor but after a short time, response for ISFET sensor does not obey the linearity. This is because as the sensors begin to capture the analyte particles available very close to the surface and the response for both ISFET and Si-NW sensor varies linearly with time. Once the region near the surface is depleted of DNA strands, the diffusion-limited transport of DNA through water molecules dictates sensor response which is proportional to $t^{1/2}$ for a 1D planar sensor and t^{1} for cylindrical sensor as seen from equation 4.2.9 and 4.2.10

Figure 5.2.7 presents the numerical results obtained by solving equation 4.1.1 and 4.1.2 using BioSensorLab. The result shows the density of captured target molecules as a function of time for both Si-NW (green) and ISFET (red) sensors and supports the analytical results presented in fifure 5.2.6.

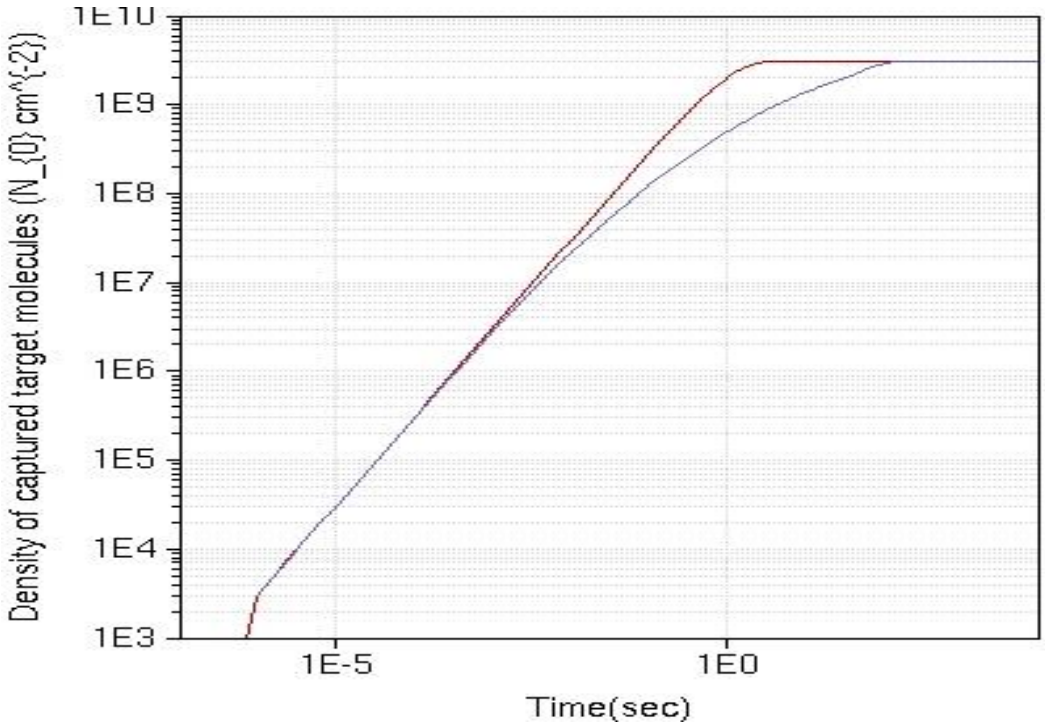

Figure 5.2.7: Comparison of sensor response between ISFET and Si-NW sensor at 100 fM analyte concentration (numerical simulation).

The results discussed above are based on the Diffusion-Capture model which does not account for the electrostatic screening of ions present in the electrolyte solution. Electrostatic screening is the damping of electric field caused by the presence of mobile charge carriers in a fluid. The above results indicate that response of a Si-NW sensor varies linearly with time. But to get actual response of 2D cylindrical sensor one must account for the factors (ion concentration in the solvent, pH of the solution etc.), that greatly affect the response of 2D cylindrical nanobiosensor. Thus taking electrostatic screening under consideration one might find that, sensitivity shows some unexpected behavior.

Figure 5.2.8 shows that sensitivity improves as target molecule density increases. The ratio of the reaction coefficients (k_F/k_R) is taken as $3x10^8$. Water is considered as the surrounding medium. Dielectric constant of water is $\varepsilon_w = 80\varepsilon_0$ and dielectric constant of the oxide layer (SiO_2) is $\varepsilon_{OX} = 3.9\varepsilon_0$. For all cases the receptor density on the sensor surface is taken 10^{12} (cm^{-2}). The ion concentration is taken 10^{-3}M. The graph shown in Figure 5.2.8 clearly shows that due to the electrostatic screening of ions in the solvent minimum detectable concentration cannot be achieved in the desired level. Figure 5.2.9 shows the result obtained from BioSensorLab that numerically solves the equations 4.2.21 and 4.2.25 simultaneously. The result presented in figure 5.2.9 shows the logarithmic dependency of sensitivity on analyte concentration and makes the analytical model (equation 4.2.28) valid. Although the analytical result shows linear dependence on target molecule density, the two results match very well. From the result shown in figure 5.2.9 one can easily predict the range of analyte concentration over which log dependency is observed. The ratio of maximum to minimum analyte concentration over which log dependency is observed is about 10^3.

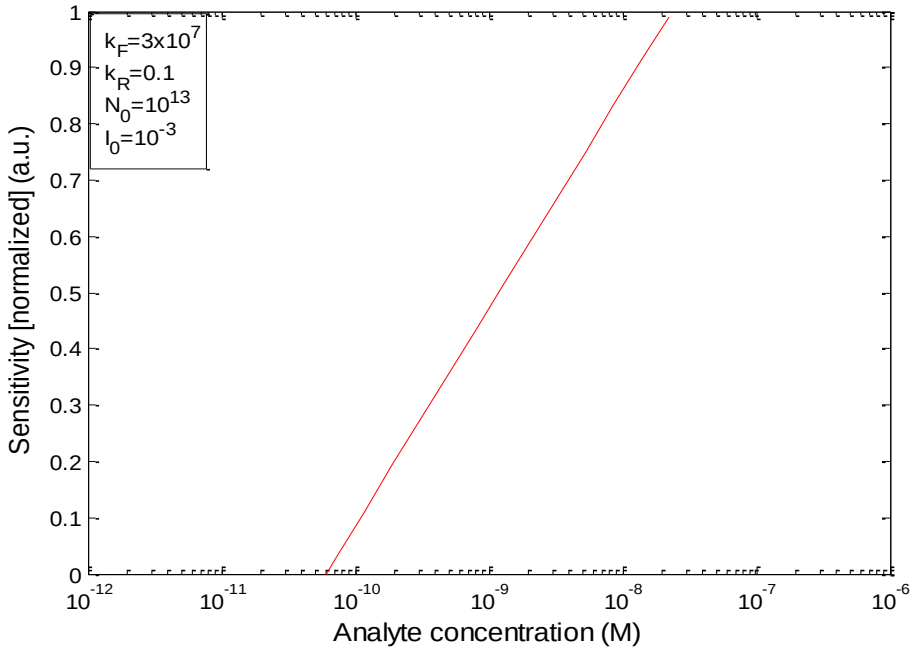

Figure 5.2.8: Sensitivity versus analyte concentration for constant ion concentration (10^{-3} M) (analytical result).

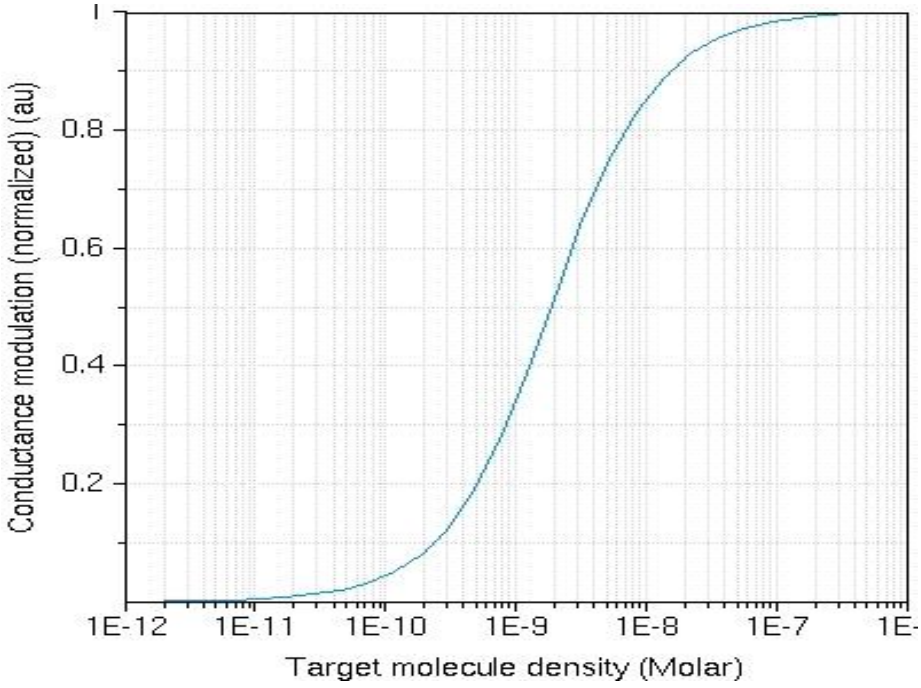

Figure 5.2.9: Sensitivity versus analyte concentration for constant ion concentration (10^{-3} M) (numerical result).

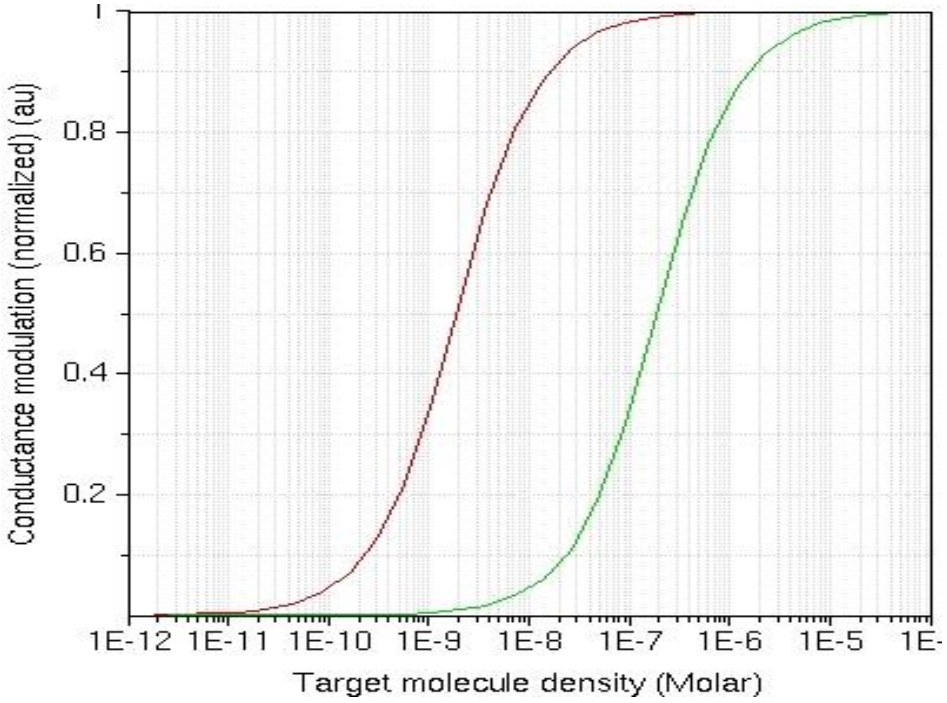

Figure 5.2.10: Sensitivity versus analyte concentration for two different $\mathbf{k_F/k_R}$ ratios (numerical simulation).

Figure 5.2.10 shows the logarithmic dependency of sensitivity on analyte concentration for two different $\mathbf{k_F/k_R}$ ratios: $3x10^8$ (red) and $3x10^6$ (green). It is seen that $\mathbf{k_F/k_R}$ ratio must be high enough to detect low analyte concentration. By comparing the two curves one may easily predict that the maximum analyte concentration for which log dependency is observed is approximately equal to the inverse of the $\mathbf{k_F/k_R}$ ratio.

Figure 5.2.11 shows the dependence of sensitivity on ion-concentration. The result is obtained by solving the analytical equation 4.2.28 at analyte concentration 10^{-9}M and $\mathbf{k_F/k_R}$ ratio $3x10^8$. It is obvious from figure 5.2.11 that sensitivity decreases with increasing ion concentration. This is reasonable because screening by the ions reduces the overall charge effective in modulating sensor response.

For the same parameters numerical result produced by the simulation tool (BioSensorLab that numerically solves the equation 4.2.21 and 4.2.25 simultaneously) is shown in Figure 5.2.12. Again the numerical result shows the logarithmic dependence of sensitivity on ion-concentration that is predicted by the analytical model developed (equation 4.2.28). Also the numerical result supports the analytical result very well.

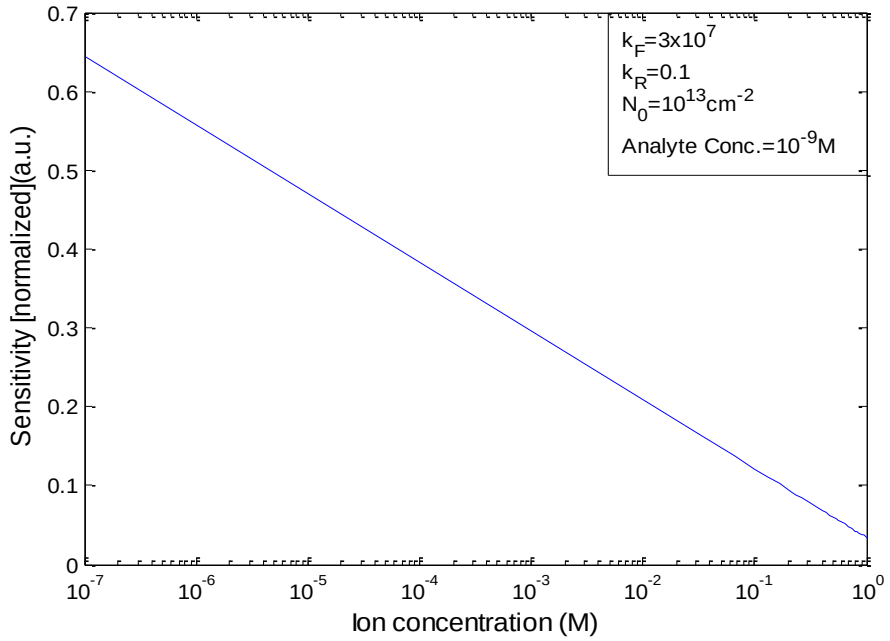

Figure 5.2.11: Sensitivity changes with ion concentration (analytical simulation).

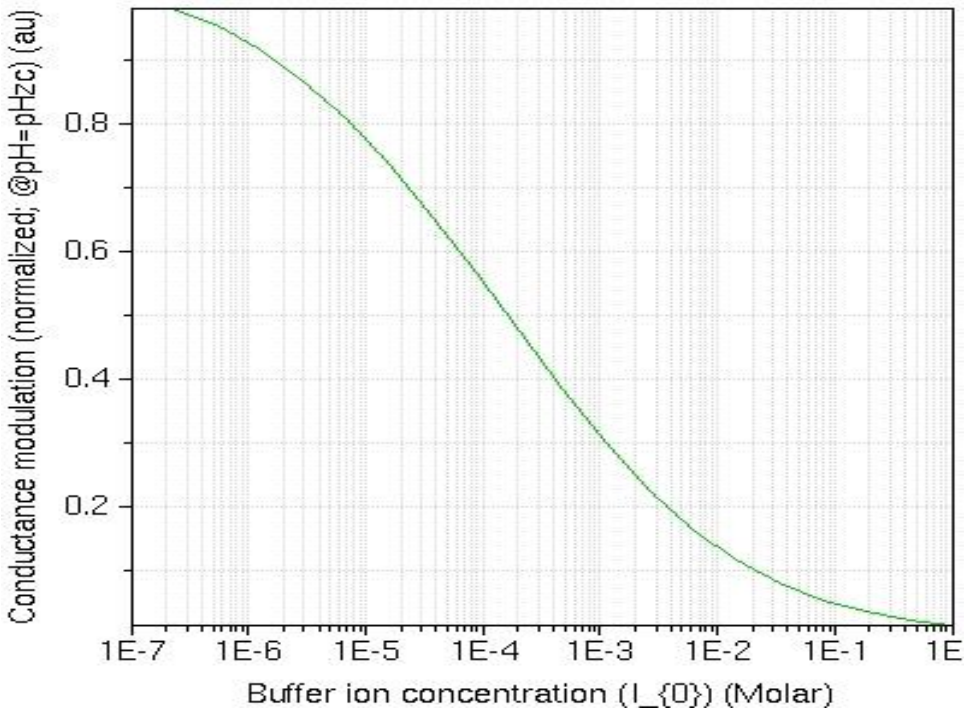

Figure 5.2.12: Sensitivity varies logarithmically with ion concentration (numerical simulation).

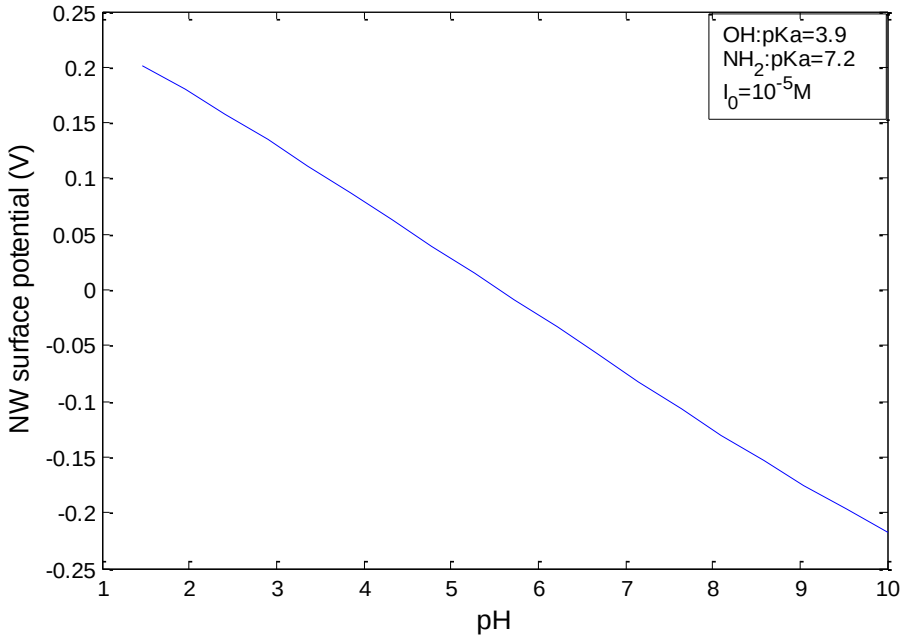

Figure 5.2.13: NW surface potential versus pH of electrolyte solution (analytical simulation).

Figure 5.2.13 shows nanowire surface potential changes linearly with pH of the solution. This study is based on the first order chemical kinetics of bond dissociation for the functionalization groups of –OH and –NH_2. For –OH and –NH_2 groups, pKa values are taken 3.9 and 7.2 respectively. Ion concentration is kept constant (10^{-5}M). The density of surface functionalization groups is considered 10^{14} (cm^{-2}). As can be seen surface potential decreases as pH of the solution increases. This is obvious because high pH of the solution means the high concentration of –OH ion in the solution and high ion concentration lower the surface potential by decreasing the charge effective in conductance modulation. The slope of the line gives the rate of change of surface potential with pH (~45mV/pH).

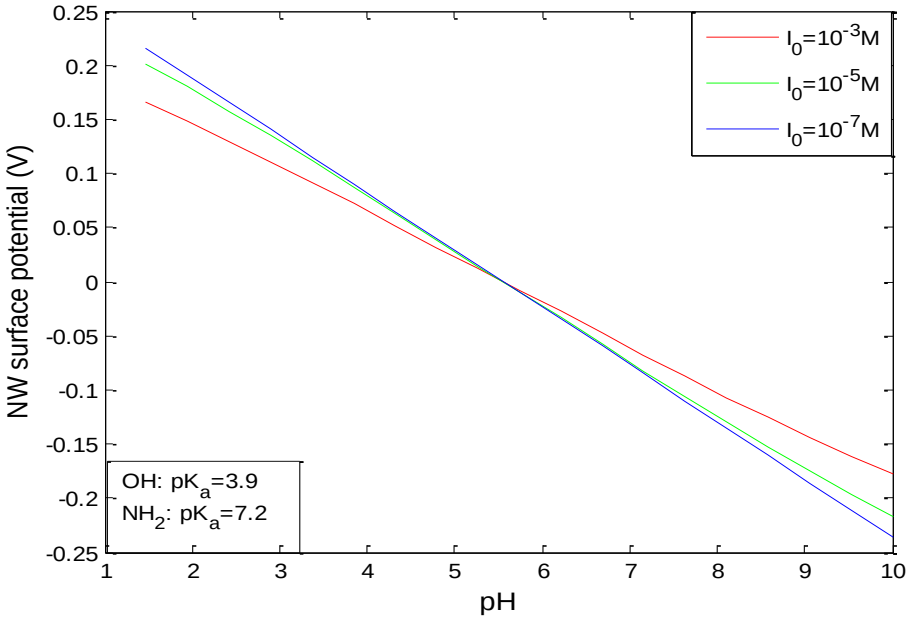

Figure 5.2.14: NW surface potential versus pH of electrolyte solution for three different ion concentrations (analytical simulation).

Figure 5.2.14 shows the change in surface potential with pH of the electrolyte solution at three different ion concentrations (10^{-3}M, 10^{-5}M and 10^{-7}M). It is seen that at higher pH value surface potential increases with ion concentration but at lower pH value it slightly reduces with ion concentration. This is because low pH means low concentration of –OH and high pH means high concentration of –OH ion in the solution. From the figure it is investigated that at a particular value of pH surface potential is zero but when the pH value decreases or increases from that value surface potential changes quickly with pH. Therefore for better sensitivity biomolecule detection should be done at pH away from this particular value.

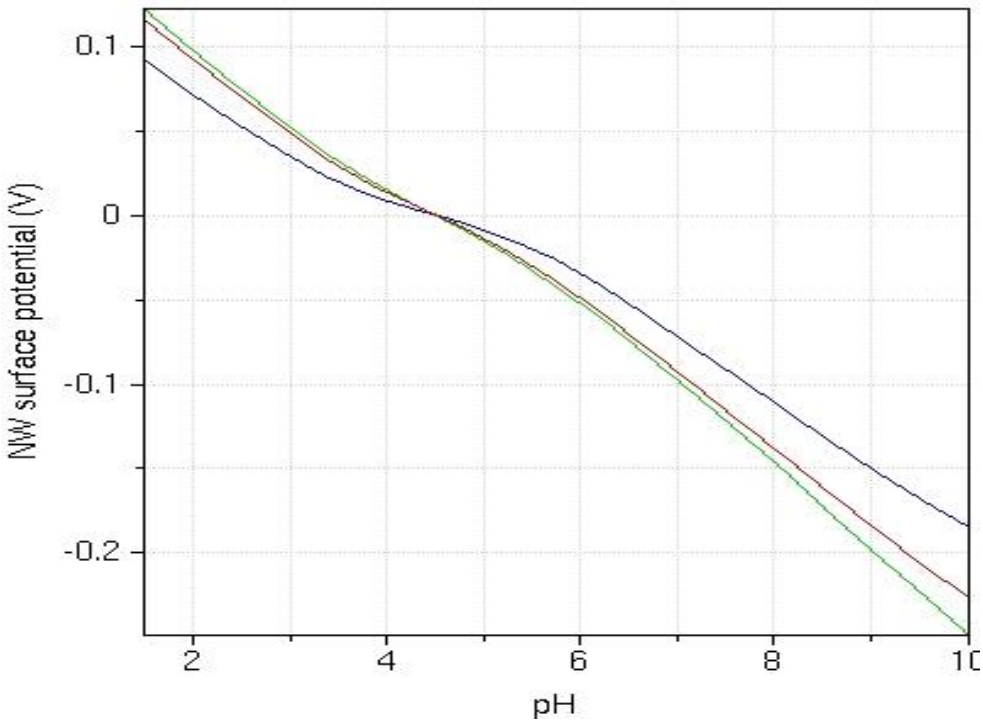

Figure 5.2.15: NW surface potential versus pH of electrolyte solution for three different ion concentrations (numerical simulation).

Figure 5.2.15 shows the variation of NW surface potential with pH of the electrolyte solution at three different ion concentrations: 10^{-7}M (green), 10^{-5}M (red) and 10^{-3}M (blue). The results are obtained by numerically solving equation 4.2.21 and 4.2.25 using the simulation tool BioSensorLab. The numerical results are well matched with the results obtained from analytical simulation using MATLAB. The analytical simulation gives the linear responses with pH. The numerical results show that, linear response can be obtained over a wide range of pH and hence validate the analytical model.

5.3 DISCUSSION

First, this analysis makes a comparison between the sensor response time and minimum detectable concentration of target biomolecules and shows nanoscale biosensors can detect upto a certain limit. This analysis investigates the detection limits for both Si-NW and planar ISFET nanosensors under same response time and shows that with 500 sec incubation time Si-NW sensor can detect upto several hundred femtomolar analyte solution whereas nanoscale ISFET sensor can detect only nanomolar concentration.

Second, the study investigates the transient response for both 2D cylindrical Si-NW and 1D planar ISFET sensors and explains why it is possible to achieve ultrafast detection by Si-NW sensor. The simulation result (Figure 5.2.6) shows the transient response of Si-NW sensor is linear whereas the transient response for ISFET sensor shows nonlinearity. Therefore, biomolecule conjugation for Si-NW sensor reaches equilibrium much before than for ISFET sensor and result is the faster response of Si-NW sensors.

Third, the model based on Poisson-Boltzmann equation developed in this thesis investigates the effects of fluidic environment (ion concentration in the solvent, pH of the solution etc.) on sensor response. The simulation result (Figure 5.2.8) shows that due to the electrostatic screening of ions in the solvent desired sensitivity cannot be achieved. This effect can be explained by the numerical result (Figure 5.2.9) obtained from simulation tool BioSensorLab, which shows the logarithmic dependency of sensitivity on target molecule density. The simulation result (Figure 5.2.10) also investigates that; reaction coefficient has a great effect on sensitivity. As it is predicted that upper bound of target molecule density for which logarithmic dependence of sensitivity is observed is approximately equal to the inverse of the $\mathbf{k_F/k_R}$ ratio, one may easily choose the analyte concentration for high sensitivity detection of biomolecules. Also the simulation result (Figure 5.2.12) explains how screening by the ions in the solvent reduces the overall sensitivity of a Si-NW biosensor.

Finally, the simulation study done in this thesis shows the effect of pH on sensor response and measure the rate of change of surface potential with pH (~45mV/pH). The simulation result (Figure 5.2.14) shows high sensitivity cannot be achieved at a particular value of pH and therefore for better sensitivity detection of biomolecules one must concern about the pH of the solution.

Chapter 6

CONCLUSION

6.1 CONCLUSION

Since the early 1970 when the ISFET was first demonstrated, the development of advanced biological sensors could impact significantly in the areas of genomics, proteomics, biomedical diagnostics and drug discovery. In this regard, nanoscale sensors based on nanowires, nanotube and other nanomaterials have received considerable attention for the charge based label free biomolecule detection. Among various nanoscale sensors Si-NW biosensors can provide direct, label free, high sensitive and high throughput analysis of biological processes and are gaining importance due to their large potential in commercial applications, ranging from detection of protein, virus and DNA to the discovery of new drug delivery systems.

Lack of fundamental theory to account for the underlying mechanism of electrical sensing of biomolecules hinders the design, optimization and development of the Si-NW Biosensor. In this work, a comprehensive modeling theory and simulation approach is presented to account for the underlying detection mechanism of ssDNA/dsDNA binding using Si-NW biosensor. The theory is based on diffusion equation and Poisson Boltzmann equation. The Poisson Boltzmann equation is derived from the classical Poisson equation using the Boltzmann distribution to model the charge distribution in the ionic solvent. The analytical and numerical solutions to the Poisson Boltzmann equation are discussed.

The detailed structures, modeling procedure and simulation methods of the Si-NW biosensor are presented. The simulation results are analyzed and the influence of parameters like the dimension of the Si-NW (diameter and length), the doping level of the Si-NW, and surrounding environment (the ions concentration in the solvent, pH of the solution etc.) are investigated for the performance optimization of the Si-NW biosensor.

At the first stage of this simulation study the performance was really frustrating as the simulation results showed ambiguous properties. This is because of the incorrect understanding of dielectric constants for the electrolyte (water) and oxide layer (SiO_2). After rigorous study and careful investigation it was realized that the dielectric constant of water should be $80\varepsilon_0$ not 80 and dielectric constant of SiO_2 should be $3.9\varepsilon_0$ not 3.9, where ε_0 is the magnetic permittivity in the free space. Also the net charge of the biomolecule (DNA) should be carefully calculated.

The modeling procedure and simulation methods shown in this work can be readily modified and adopted for detection of other receptor-target biomolecules pairs, such as biotin-Streptavidin, antibody-protein and antibody-virus, using Si-NW biosensor. Both numerical and analytical simulation results indicate that the optimal sensor performance can be ensured by careful optimization of its parameters. In addition such optimization is essential for integrating the silicon nanowires into electrically addressable sensor arrays for multiplexed detection.

As a conclusion, to design highly sensitive biosensor using Si-NW one must systematically optimize sensor response as a function of sensor geometry, fluidic conditions, and the ion concentration in the aqueous solution. And Si-NW biosensor has huge potential that can be exploited to be an efficient electronic sensing device in the biocommercial applications.

6.2 FUTURE WORK

Investigating the performance parameters of Si-NW biosensor is very enthusiastic since the device has many aspects that can be explored and improved. The model developed in this thesis investigates the detection limits of the charged biomolecules only. Detection of neutral biomolecules using sensors based on nanostructures is still a promising target to the researchers of biosensor. One possible solution for neutral biomolecule detection may be the improvement of the functionalization scheme by producing highly charged artificial receptor molecules in nanoscale and then immobilized on the sensor surface.

In this work, only the static binding of ssDNA/dsDNA molecules is considered and all the target molecules are assumed to bind at the center of Si-NW. However, the real case is not much like that. The target bimolecule diffuses in the electrolyte and bind to the receptors at random location and with random binding angle. This binding is a stochastic process and can be simulated using a Monte Carlo algorithm.

The response of a Si-NW sensor is affected by the electrostatic screening of the ions in the solvent. In this thesis the simulation study shows that the optimal response can be achieved by careful optimization of parameters: sensor geometry, fluidic conditions, and the ion concentration in the aqueous solution. One possible solution to reduce the electrostatic screening may be, use of extra bias to introduce current in the electrolyte solution since application of bias voltage in an ionic solution reduces the screening equivalent capacitance.

Besides, the outcome of simulation analysis in this thesis is based on ideal condition of Si-NW, an experimental work including the fabrication process of Si-NW sensor will provide more realistic results.

APPENDIX A: GAUSS'S LAW

In physics, Gauss's law is a law relating the distribution of electric charge to the resulting electric field. In free space or vacuum, Gauss's law may be expressed in its differential form:

$$\nabla . \overrightarrow{E} = \frac{\rho}{\varepsilon_0} \tag{A1}$$

Where $\nabla .$ denotes divergence, $\overrightarrow{E}$ is the electric field, and ρ is the total electric charge density (including both free and bound charge), and ε_0 is the permittivity in vacuum. Using the relation:

$$\overrightarrow{E} = -\nabla\varphi \tag{A2}$$

where Φ is the scalar potential and ∇ denotes gradient operation, equation (A1) can be rewritten as:

$$\nabla . \nabla\varphi = \nabla^2\varphi = -\frac{\rho}{\varepsilon_0} \tag{A3}$$

This equation is called Poisson equation. In region of space that lacks a charge density, this equation becomes Laplace equation:

$$\nabla^2\varphi = 0 \tag{A4}$$

In a dielectric, the differential form of Gauss' law is then given by the following equations:

$$\nabla . \vec{D} = \rho \tag{A5}$$

$$\vec{D} = \varepsilon_0\vec{E} + \vec{P} \tag{A6}$$

where $\vec{D}$ is electric displacement vector and $\vec{P}$ is the polarization vector. In linear dielectric, the polarization $\vec{P}$ becomes zero, and equation (A5) becomes:

$$\vec{D} = \varepsilon_0 \vec{E} \tag{A7}$$

The dielectric constant or relative permittivity ε_r is defined as the ratio of the permittivity in the dielectric, ε, to the permittivity in vacuum, ε_0:

$$\varepsilon_r = \frac{\varepsilon}{\varepsilon_0} \tag{A8}$$

Finally, the differential form of Gauss' law for a linear dielectric can be written as:

$$-\nabla.(\varepsilon \nabla \varphi) = \rho \tag{A9}$$

A detailed derivation of the Gauss' law in both free space and in a dielectric can be found in [34].

APPENDIX B: BOLTZMANN DISTRIBUTION

In physics, the Boltzmann distribution is a certain distribution or probability measure of a system of particles among the various energy states. For a system of N ($N = \sum_i n_i$) particles, the Boltzmann distribution gives the most probable distribution of finding n_1 particles with energy u_1 , n_2 particles with energy u_2, and so on.

The Boltzmann distribution can be derived using the assumption of distinguishable particles. Suppose there is a number of energy levels, labeled by index *i* (*i* =1, 2,…k), each energy level having energy u_i and containing n_i particles. Then use $\boldsymbol{W}$ to denote the number of ways of distributing n_i particles with energy u_i. In this derivation, ignoring the degeneracy problem, means that, there is only one way to put particles into energy level *i*. Then N particles can be distributed in the following orders: selecting n_1 particles from N particles and placing them in energy level 1; then selecting n_2 particles from remaining $N - n_1$ particles and placing them in energy level 2; continuing this process until all particles are distributed. It can be easily seen that the number of ways of selecting objects from N objects without regard to order is:

$$C_{n_1}^{N} = \frac{N!}{n_1!(N-n_1)!} \tag{B1}$$

Similarly, the number of ways of selecting n_2 objects from $N - n_1$ particles without regard to order is:

$$C_{n_2}^{N-n_1} = \frac{(N-n_1)!}{n_2!(N-n_1-n_2)!} \tag{B2}$$

So $\boldsymbol{W}$ can be calculated as:

$$W = C_{n_1}^{N} C_{n_2}^{N-n_1} \dots C_{n_k}^{n_k} = \left(\frac{N!}{n_1!(N-n_1)!}\right)\left(\frac{(N-n_1)!}{n_2!(N-n_1-n_2)!}\right)\dots\left(\frac{n_k!}{n_k!0!}\right) = \frac{N!}{n_1!n_2!\dots n_k!} \tag{B3}$$

To find a set of n_i to maximize $\boldsymbol{W}$ subject to the constraint that the number of particles and energy level are fixed. Since maxima of $\boldsymbol{W}$ and ln($\boldsymbol{W}$) can be obtained by the same value of n_i, for simplicity in mathematics, ln($\boldsymbol{W}$) is maximized instead of maximizing $\boldsymbol{W}$. To

maximize ln(***W***) subject to the constraint of the number of particles and energy level, a function can be constructed using the method of Lagrange multipliers as:

$$f(n_1 n_2 \dots n_k) = \ln(W) + \alpha(N - \sum_i n_i) + \beta(E - \sum_i n_i u_i) \quad \text{(B4)}$$

where the last term on the right hand side shows the conservation of total energy. From equation (B3), $\ln(W)$ is found as:

$$\ln(W) = \ln(N!) - \sum_i \ln(n_i!) + \sum_i (n_i ln g_i) \quad \text{(B5)}$$

Using Stirling's formula [35], for large N,

$$N! \approx N^N e^{-N} \quad \text{(B6)}$$

then,

$$\ln(N!) \approx N ln N - N \quad \text{(B7)}$$

also noticing that, $N = \sum_i n_i$ then,

$$ln W = N ln N - \sum_i (n_i ln n_i) + \sum_i (n_i ln g_i) \quad \text{(B8)}$$

finally,

$$f(n_1 n_2 \dots n_k) = N ln N + \alpha N + \beta E + \sum_i (n_i ln g_i - n_i ln n_i - (\alpha + \beta \mu_i) n_i) \quad \text{(B9)}$$

In order to maximize the above equitation, the partial derivative of function ***f*** with respect to n_i should be zero:

$$\frac{\partial f}{\partial n_i} = ln g_i - ln n_i - (\alpha + \beta \mu_i) = 0 \quad \text{(B10)}$$

By solving the above equation, and noticing thermodynamically that $\beta = 1/(k_B T)$ where k_B is the Boltzmann's constant and T is the absolute temperature of the system, then the expression for n_i:

$$n_i = n_\infty \exp\left(-\frac{u_i}{k_B T}\right) \tag{B11}$$

This is the well known Boltzmann distribution. Here, n_∞ is the mean distribution at far-field [35]. More details on the derivation of the Boltzmann distribution can be found in [36] and [37].

APPENDIX C: CODING

LISTING 1: MATLAB SOURCE CODES FOR SIMULATION OF NW SENSITIVITY AS FUNCTION OF RADIUS

```
%Sensitivity of nanowire biosensor varies with nanowire radius
%Sunday, August 19,2012.
%Program runs by Obaed

q = 1.6e-19;
N_t = 1e9;
N_d =[1e17 1e18 1e19];
Sig_s = 24*1.6e-19;



a_0 = 1e-6 : (4e-6 - 1e-6) / 300 : 4e-6;

sensitivity_1 = ((2*Sig_s* N_t)/(q*N_d(1)))./a_0;
plot (a_0 ,sensitivity_1, 'linestyle' , '-' , 'color' , 'r','linewidth',[1]
)
hold on

sensitivity_2 = ((2*Sig_s* N_t)/(q*N_d(2)))./a_0;
plot (a_0 ,sensitivity_2, 'linestyle' , '-' , 'color' , 'g','linewidth',[1]
)
hold on

sensitivity_3 = ((2*Sig_s* N_t)/(q*N_d(3)))./a_0;
plot (a_0 ,sensitivity_3, 'linestyle' , '-' , 'color' , 'b','linewidth',[1]
)


xlabel ( 'Radius(nm)','fontsize',[12] ) ;
ylabel ( 'sensitivity','fontsize',[12] ) ;
legend ('N_d=10^{17}' ,'N_d=10^{18}' ,   'N_d=10^{19}','fontsize',[12]) ;
```

LISTING 2: MATLAB SOURCE CODES FOR SIMULATION OF SETTLING TIME AS FUNCTION OF ANALYTE CONCENTRATION

```
%Sensor response time for femtomolar detection.
%Sunday, August 12, 2012.
%Program runs by Obaed.

a_0 = 3e-6;
N_s = 10e-12;
bp =12;
D = 4.9e-6/bp^0.72;

rho_0 = 1e-14 : (4e-6 - 1e-14) / 300 : 4e-6;
```

```
settling_time_1 = (2*N_s^2/D)./(rho_0.^2);
plot (rho_0 ,settling_time_1, 'linestyle' , '-' , 'color' ,
'g','linewidth',[1] )
hold on


settling_time_2=ones(1,length(rho_0)); % initial value
settling_time_2_old=zeros(1,length(rho_0));
err=1;

while err>1e-6

settling_time_2 =
(N_s*a_0*log10(((4*D.*settling_time_2).^.5+a_0)/a_0)/D)./rho_0;

diff=settling_time_2_old-settling_time_2;

err=sum(abs(diff));

settling_time_2_old=settling_time_2;

end


plot (rho_0 ,settling_time_2, 'linestyle' , '-' , 'color' ,
'r','linewidth',[1] )

hold on
h_line=500*ones(1,length(rho_0));
plot (rho_0 ,h_line, 'linestyle' , '-' , 'color' , 'b','linewidth',[1] )


xlabel ( 'Analyte concentration(molar unit)','fontsize',[12] ) ;
ylabel ( 'Settling time(sec)','fontsize',[12] ) ;
legend ('Planar ISFET' ,'Cylindrical NW') ;
```

LISTING 3: MATLAB SOURCE CODES FOR SIMULATION OF TRANSIENT RESPONSE OF TWO TYPES OF BIOSENSORS

```
%Transient response for two types of Biosensors.
%Monday, September 3, 2012.
%Program runs by Obaed

a_0 = 3e-6;
bp = 12;
D = 4.9e-6/bp^0.72;
N_0 = 1e13;
K_f = 3e7;
rho_0 = 1e-13;


t = 1e-6 : (1e4 - 1e-6) / 300 : 1e4;
```

```
N_t_1 = ones(1,length(t)); % initial value
N_t_1_old = zeros(1,length(t));
err = 1;

while err>1e-6

N_t_1 = (rho_0.*t) / (((a_0.*log10(((4*D.*t).^.5+a_0)/a_0))/D)+
(1/(K_f*N_0)));
diff = N_t_1_old - N_t_1;

err = sum(abs(diff));

N_t_1_old = N_t_1;

end


plot (t ,N_t_1, 'linestyle' , '-' , 'color' , 'g','linewidth',[1] )
hold on

N_t_2 = ones(1,length(t)); % initial value
N_t_2_old = zeros(1,length(t));
err=1;

while err>1e-6

N_t_2 = (rho_0.*t) / (((2.*t)/D).^.5 + (1/(K_f*N_0)));
diff = N_t_2_old - N_t_2;

err = sum(abs(diff));

N_t_2_old = N_t_2;

end


plot (t ,N_t_2, 'linestyle' , '-' , 'color' , 'r','linewidth',[1] )

xlabel ( 'time(sec)','fontsize',[12] ) ;
ylabel ( 'Density of captured target molecules N(t)(cm^{-
2})','fontsize',[12] ) ;
legend ('Cylindrical NW' ,'Planar ISFET' ,   'fontsize',[12]) ;
```

LISTING 4: MATLAB SOURCE CODES FOR SIMULATION OF SENSITIVITY AS FUNCTION OF ION CONCENTRATION

```
%Sensitivity Changes with ion concentration
%Monday, September 17, 2012.
%Program runs by Obaed

q = 1.6e-19;
T = 300;
K_b = 1.38e-23;
B = q/(K_b*T);
D = 1.6e-4;
a_0 = 30e-9;
N_d = 1e25;
N_0 = 1e17;
K_f = 3e7;
K_r = 0.1;
N_avo = 6.022e23;
Eps_ox = 3.9*8.854e-12;
Eps_w = 80*8.854e-12;
t_ox = 1e-9;
Sig_s = 24*1.6e-19;

rho_0 = 1e-9;

I_0 = 1e-7 : (1e0 - 1e-7) / 30 : 1e0;


C_2 = log (((Sig_s * K_f*N_0)/K_r)*( B / (2 * q * Eps_w * N_avo) )^1/2  );
C_1 = (4 * Eps_ox) / ( B * q * a_0^2 * N_d * log(1 + t_ox / a_0) );
S = C_1 * ( log(rho_0)  - log(I_0) / 2 + C_2);

plot (I_0 ,S, 'linestyle' , '-' , 'color' , 'b','linewidth',[1] )


xlabel ( 'Ion concentration (M)','fontsize',[12] ) ;
ylabel ( 'Sensitivity [normalized](a.u.)','fontsize',[12] ) ;
```

LISTING 5: MATLAB SOURCE CODES FOR SIMULATION OF SENSITIVITY AS FUNCTION OF pH OF THE ELECTROLYTE SOLUTION

```
%NW surface potential depends on the pH of the electrolyte solution.
%Monday, September 17, 2012.
%Program runs by Obaed

q = 1.6e-19;
T = 300;
K_b = 1.38e-23;
B = q/(K_b*T);

a_0 = 30e-9;
N_d = 1e25;
N_f = 1e18;
pKa = 11.1;


N_avo = 6.022e23;
Eps_ox = 3.9*8.854e-12;
Eps_w = 80*8.854e-12;
t_ox = 1e-9;
I_0 = 1e-5;


pH = 1 : (10 - 1) / 30 : 10;

C_2 = log(  (  (2*  Eps_w * N_avo)/(q * B * N_f^2) )^1/2) ;
surface_potential = (2/B)*( -2.303*(pH-pKa) + log(I_0) / 2 + C_2);
plot(Ph ,surface_potential,'linestyle' ,'-' ,'color' ,'b','linewidth',[1] )


xlabel ( 'pH','fontsize',[12] ) ;
ylabel ( 'NW surface potential(V)','fontsize',[10] ) ;
```

REFERENCES

[1]. P. R. Nair, and M. A. Alam, "Design considerations of silicon nanowire biosensors", *IEEE TRANSACTIONS ON ELECTRON DEVICES*, 54 (12), Dec. 2007.

[2] P. Bergveld, "Development, operation and application of the ion sensitive field effect transistor as a tool for electrophysiology", *IEEE Trans. Biomed. Eng. BME-19,* pp. 342–351, 1972.

[4] C. Heitzinger, and G. Klimeck, "Computational aspects of the three-dimensional feature-scale simulation of silicon-nanowire field-effect sensors for DNA detection", *Journal of Computational Electronics*, 6:387-390, 2007.

[4] S. J. Han, H. Yu, R. J.Wilson, R. L. White, N. Pourmand, and S. X.Wang, "CMOS integrated DNA Microarray based on GMR sensors," *IEDM Tech. Dig.,* pp. 719–723, 2006.

[5] P. Bergveld, "Thirty years of ISFETOLOGY—What happened in the past 30 years and what may happen in the next 30 years," *Sens. Actuators B, Chem.*, vol. 88, no. 1, pp. 1–20, Jan. 2003.

[6] R. J. Lipschutz, S. P. A. Fodor, T. R. Gingeras, and D. J. Lockhart, "High-density synthetic oligonucleotide arrays," *Nat. Genet.*, vol. 21, pp. 20–24,1999.

[7] Z. Li, B. Rajendran, T. I. Kamins, X. Li, Y. Chen, and R. S. Williams, "Silicon nanowires for sequence-specific DNA sensing: Device fabrication and simulation," *Appl. Phys. A, Solids Surf.*, vol. 80, no. 6, pp. 1257–1263, Mar. 2005.

[8] J. Wang, D. Palecek, P. E. Nielsen, G. Rivas, X. Cai, H. Shiraishi, N. Dontha, D. Luo, and P. A. M. Farias, "Peptide nucleic acid probes for sequence-specific DNA biosensors," *J. Amer. Chem. Soc.*, vol. 118, no. 33, pp. 7667–7670, 1996.

[9] P. E. Sheehan and L. W. Whitman, "Detection limits for nanoscale biosensors," *Nano Lett.*, vol. 5, no. 4, pp. 803–806, 2005.

[10] M. Pohanka and P. Skladal, "Electrochemical biosensors – principles and applications*" J. Appl. Biomed. **6**:* 57–64, ISSN 1214-0287, 2008.

[11] M.Yuqing, G. Jianguo, C. Jiranrong, "Ion Sensitive Field Effect Transducer based Biosensor", *Biotechnology Advances*, 21, 527-534, June, 2003.

[12] M. E. Bosch, A. J. R. Sánchez, F. S. Rojas, and C. B. Ojeda, "Recent Development in Optical Fiber Biosensors" *Sensors, 7,* 797-859, May, 2007.

[13] M. F. Frasco and N. Chaniotakis "Semiconductor Quantum Dots in Chemical Sensors and Biosensors", *Sensors, 9,* 7266-7286, sept, 2009.

[14] P. R. Nair, and M. A. Alam, "Simulation of nanowire bio-sensors," in *Proc. 64th Device Res.Conf.,* pp. 183-184, 2006.

[15] P. Qi, O. Vermesh, M. Grecu, A. Javey, Q. Wang, and H. Dai, "Toward large arrays of multiplex functionalized carbon nanotube sensors for highly sensitive and selective molecular detection," *Nano Lett.*, vol. 3, no. 3, pp. 347–351, 2003.

[16] Z. Li, Y. Chen, X. Li, T. I. Kamins, K. Nauka, and R. S. Williams, "Sequence-specific label-free DNA sensors based on silicon nanowires," *Nano Lett.*, vol. 4, no. 2, pp. 245–248, 2004.

[17] P. R. Nair, and M. A. Alam, "Theory of "Selectivity" of label-free nanobiosensors: A geometro-physical perspective", *JOURNAL OF APPLIED PHYSICS*, 107,064701, Jan. 2010.

[18] M. N. Masood, S. Chen, E. T. Carlen, and A. van den Berg, *"*All-(111) Surface Silicon Nanowires: Selective Functionalization for Biosensing Applications*" American Chemical Society*, VOL. 16, NO. 12, 3422–3428, Nov. 2010.

[19] I. Park , Z. Li , A. P. Pisano, R. S. Williams, *Nano Lett., 7*, 3106, 2007.

[20] V. A. Bloomfield, D. M. Crothers, and I. Tinoco, Jr., "Nucleic Acids: Structures, Properties, and Functions". *Sausalito, CA: Univ. Sci. Books*, 2000.

[21] H. C. Berg., "*Random Walks in Biology"* Princeton University Press, Princeton, NJ, 1993.

[22] E. Stern, J. F. Klemic, D. A. Routenberg, P. N. Wyrembak, D. B. Turner-Evans, A. D. Hamilton, D. A. LaVan, T. M. Fahmy, and M. A. Reed, "Label-free immune-detection with CMOS-compatible semiconducting nanowires," *Nature*, vol. 445, no. 7127, pp. 519–523, Feb. 2007.

[23] P. Bergveld, R. E. G van Hal, J. C. T. Eijkel, *Biosens. Bioelectron. 10*, 405–414, 1995.

[24] A. S. Ahmad, K. Tuncay, and P. J. Ortoleva, "Efficient solution technique for solving the poisson-boltzmann equation", *J. Comput. Chem*., 25, pp. 1068–1074,2004.

[25] *https://nanohub.org/tools/BioSensorLab*

[26] H.MBerman, J.Westbrook, Z. Feng, G. Gilliland, T. N. Bhat, H.Weissig, I. N. Shindyalov, and P. E. Bourne*, "The Protein Data Bank," Nucleic Acids Res., vol. 28, no. 1, pp. 235–242*, 2000.

[27] W. F. van Gunsteren and H. J. C Berendsen, *Biomos BV Gromos-87Manual*, 1987.

[28] J. Hahm, and C. M. Leiber, *Nano. Lett., 4*, 51–55, 2004.

[29] H. J. Ohshima, *Colloid Interface Sci., 200,* 291–298, 1998.

[30] D. McQuarrie, *Statistical Mechanics*. New York: Harper & Row, 1976.

[31] R. B. Paris, & D. Kaminsky, *Asymptotics and the Mellin-Barnes Integrals*, New York: Cambridge University Press (2001).

[32] F. Fogolari, A. Brigo, H. Molinari, "The Poisson–Boltzmann equation for biomolecular electrostatics: a tool for structural biology", *J Mol Recognit* 15(6):377–392, 2002

[33] M. Holst, "The Poisson–Boltzmann equation: Analysis and multilevel numerical solution," in "Applied Mathematics and CRPC," California Inst. Technol., Pasadena, CA, 1994. Tech. Rep.

[34] W. B. CHESTON, Elementary theory of electric and magnetic fields, John Wiley& Sons, Inc., 1964, ch. 2–5.

[35] R. S. Sampath, A Study of the Poisson-Boltzmann Equation and its Applications in the Sensitivity Analysis of VCP/SPICE, http://www.cc.gatech.edu/~rahulss/index_files/indRepFinal.pdf

[36] P. Atkins and J. W. Locke, *Atkins' Physical Chemistry*, Oxford University Press; 7th edition (January 2002).

[37] http://en.wikipedia.org/wiki/Maxwell%E2%80%93Boltzmann_statistics